Understanding the Surface Hopping View of Electronic Transitions and Decoherence

Joseph E. Subotnik, Amber Jain, Brian Landry, Andrew Petit, Wenjun Ouyang, and Nicole Bellonzi

Department of Chemistry, University of Pennsylvania, Philadelphia, Pennsylvania 19104; email: subotnik@sas.upenn.edu

Annu. Rev. Phys. Chem. 2016. 67:387–417

The *Annual Review of Physical Chemistry* is online at physchem.annualreviews.org

This article's doi: 10.1146/annurev-physchem-040215-112245

Keywords

nonadiabatic dynamics, measurement, electron transfer, energy transfer

Abstract

We present a current, up-to-date review of the surface hopping methodology for solving nonadiabatic problems, 25 years after Tully published the fewest switches surface hopping algorithm. After reviewing the original motivation for and failures of the algorithm, we give a detailed examination of modern advances, focusing on both theoretical and practical issues. We highlight how one can partially derive surface hopping from the Schrödinger equation in the adiabatic basis, how one can change basis within the surface hopping algorithm, and how one should understand and apply the notions of decoherence and wavepacket bifurcation. The question of time reversibility and detailed balance is also examined at length. Recent applications to photoexcited conjugated polymers are discussed briefly.

1. INTRODUCTION

When materials are subject to optical photon fields (in the range of several electron volts), electrons can absorb the light and jump into excited states. Subsequently, when the electronically excited molecules relax, there is a natural exchange of energy between electronic quantum states and nuclear motion. By energy conservation, every electronic transition downward must be accompanied by an increase in the thermal energy of nuclei (which is effectively thermal friction). This nuclear motion can in turn push molecules toward very high-energy geometries, where one might find new electronic state crossings, and the cycle continues. Molecular photochemistry and photoinduced dynamics can be very complicated.

As an example, consider the molecule 4(2-naphthylmethyl)benzaldehyde (shown in **Figure 1**), which was studied experimentally by Piotrowiak, Closs, and coworkers (1, 2) (with the substitution of benzaldehyde for benzophenone). After photoexcitation to the S_1 excited state, the molecule quickly (in a few picoseconds) undergoes intersystem crossing into the T_2 triplet state followed by internal conversion to the T_1 state (20 ps). The $T_2 \rightarrow T_1$ conversion proceeds via a conical intersection where a triplet exciton transfers from benzophenone to naphthalene. Thereafter, relaxation to the ground state is slow and nonradiative. The goal of surface hopping dynamics is to characterize the flow of energy through photoexcited systems like these (3).

The surface hopping algorithm can be implemented on the fly with ab initio electronic structure theory, provided that one can solve the electronic Schrödinger equation and compute the relevant potential energy surfaces and derivative couplings (4, 5). If one has this capability, surface hopping dynamics can be used to study coupled nuclear–electronic dynamics over fairly long time scales. The surface hopping algorithm is one of only a few practical approaches for solving such coupled dynamics for large, condensed phase systems. Other options include Ehrenfest dynamics (6) [best when symmetrized and quasi-quantized (7)] and multiple-spawning dynamics (8, 9).

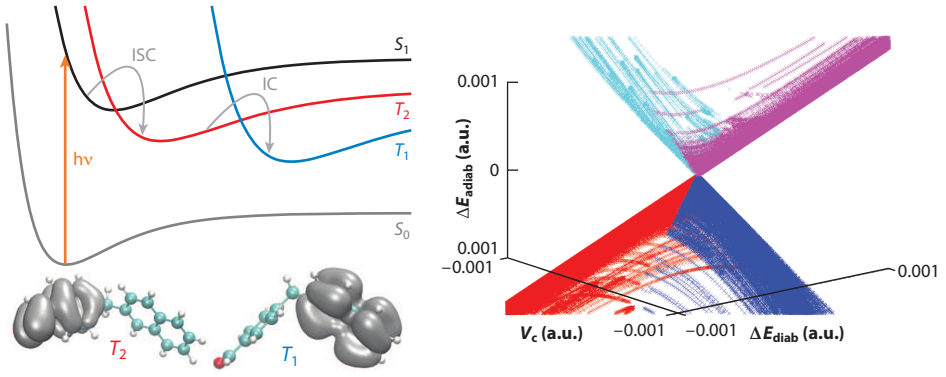

Figure 1

Closs's (1, 2) M molecule [4(2-naphthylmethyl)benzaldehyde]. (*Left*) After photoexcitation to S_1 with a photon of energy $h\nu$, there is an intersystem crossing (ISC) to T_2, followed by internal conversion (IC) through a conical intersection to T_1. (*Right*) A $T_2 \rightarrow T_1$ conical intersection was identified directly from surface hopping dynamics (3): The dynamics access nuclear geometries where both the diabatic coupling (V_c) and the diabatic energy difference (ΔE_{diab}) are zero, so that $\Delta E_{adiab} = 0$. The four colors correspond to donor/acceptor diabatic character associated with the lower/upper adiabatic surface: red = donor/lower; blue = acceptor/lower; cyan = donor/upper; purple = acceptor/upper. The $T_2 \rightarrow T_1$ transition represents an energy transfer event, with an exciton hopping from the donor (benzaldehyde) to the acceptor (naphthalene). Surface hopping calculations can replicate this photophysics (3).

An outline of this review is as follows. In Section 2, we give a brief overview of quantum dynamics as relevant for nonadiabatic problems, highlighting exact versus approximate algorithms. This leads us to John Tully's (10) approximate fewest switches surface hopping (FSSH) algorithm, which was originally hypothesized rather than derived. In Section 3, we highlight some of the early problems with surface hopping, both practical and theoretical, that limited the utility of the algorithm. In Section 4, we introduce several important recent advances vis-à-vis the surface hopping algorithm, advances that have grounded the FSSH algorithm in modern theoretical chemistry. Major benchmarking results are given in Section 5. In Section 6, we discuss in detail one of the most contentious aspects of the FSSH algorithm, namely the question of detailed balance and time reversibility. We conclude in Section 7. Our choice of topics is not meant to be exhaustive. The reader can find other reviews of surface hopping in References 11–16.

1.1. Notation

For simplicity of notation, in this article we consider systems with either one or two electronic states (e.g., the ground $|1\rangle$ and excited $|2\rangle$ states). Roman numerals index electronic degrees of freedom, the letters *ijk* index adiabatic electronic states, and the letters *abc* index diabatic electronic states. Greek letters ($\alpha\beta\gamma$) index nuclear degrees of freedom. The only exception to this rule is the active adiabatic surface, which is always denoted by λ. The mass of the α-th nuclear degree of freedom is denoted by M^{α}. Nuclear operators are denoted with a hat (e.g., $\hat{T}$), and electronic operators are in bold (e.g., $\mathbf{H}_{\mathrm{el}}$). Vectors (nuclear or electronic) sit under an arrow (e.g., $\vec{c}$).

2. NONADIABATIC DYNAMICS

2.1. Exact Trajectory Approaches for Adiabatic Nuclear Quantum Dynamics

Consider a system with N_p nuclear degrees of freedom moving along a single potential energy surface. Solving for the exact quantum dynamics of such a system is prohibitively expensive for large N_p. To solve the Schrödinger equation,

$$i\hbar\frac{\mathrm{d}|\Psi\rangle}{\mathrm{d}t} = \hat{H}\,|\Psi\rangle,$$

or the Liouville equation,

$$\frac{\mathrm{d}\hat{\rho}}{\mathrm{d}t} = \frac{-i}{\hbar}[\hat{H}\,,\hat{\rho}],$$

with a straightforward algorithm scales as N^3 (for a basis of dimension N). In principle, for reaction dynamics, one must include a grid of N_g points for every degree of freedom, so that $N \approx N_g^{N_p}$. This exponential scaling limits pure quantum dynamics to a handful of degrees of freedom.

As an alternative, if one seeks a trajectory description of quantum mechanics, one is formally forced to evaluate either a Feynman path integral or a Bohmian quantum potential. Neither is numerically stable. For a Feynman path integral, one must evaluate the propagator $\langle\vec{x}\,|e^{-i\hat{H}t/\hbar}|\vec{x}'\rangle = \int D[\vec{x}(t)]e^{iS[\vec{x}(t)]}$, summing over all the possible trajectories between two configurations and weighting every trajectory by the complex phase $e^{iS[\vec{x}(t)]}$, where S is the action. In practice, this sum rarely converges for big systems [although there has been tremendous success for the unique case of harmonic baths (17–19)].

For Bohmian dynamics, one is required to sample a nearly infinite swarm of trajectories and to build up the quantum potential:

$$Q = \frac{1}{\sqrt{\rho(\vec{x}, t)}} \sum_{\alpha} \frac{-\hbar^2}{2M^{\alpha}} \frac{\partial^2}{\partial x_{\alpha}^2} \sqrt{\rho(\vec{x}, t)}. \quad (1)$$

Here, $\rho(\vec{x}, t)$ is the wavepacket density at position $\vec{x}$. From Equation 1, one must conclude that independent trajectories are an impossibility: If a wavepacket is to be considered a swarm of classical point particles, those point particles must interact with each other as they evolve in time. Moreover, because one must divide by the density of trajectories in phase space (which will diverge near a node of the wavefunction), Bohmian mechanics is usually plagued by numerical instabilities (20).

In these methods, we already see the basic conundrum of trajectory quantum mechanics. On the one hand, dynamics can be achieved through independent trajectories, but these trajectories must carry complex weights, and this inevitably leads to instability upon averaging. On the other hand, dynamics can be achieved with positively weighted trajectories, but these trajectories cannot be independent, and to propagate one trajectory requires a large number of trajectories nearby. In many dimensions, the number of needed trajectories grows exponentially, and the number of trajectories also grows in time. Without enough trajectories, coupled trajectories are also unstable.

2.2. Semiclassical Approximations and the Meyer–Miller–Stock–Thoss Mapping for Nonadiabatic Quantum Dynamics

Over the past 50 years, this conundrum has led to a host of semiclassical dynamics with the goal of incorporating some quantum effects through classical mechanics. In particular, Miller and coworkers (21) have proposed a hierarchy of approaches for approximating thermal quantum correlation functions $\langle AB(t)\rangle = \mathrm{Tr}(\hat{\rho}\hat{A}e^{iHt}\hat{B}e^{-iHt})$ in the context of classical trajectories. Miller's hierarchy is:

1. Linearized semiclassical initial value representations (LSC-IVR), whereby one reduces the complex weights $\exp(iS(t))$ (for action $S(t)$) by linearization of forward and backward paths. In practice, one runs classical trajectories but one samples from the Wigner density and replaces quantum operators with their Wigner representations. This approach is natural and stable, but Miller (21, 22) has argued that, from his point of view, LSC-IVR carries no quantum coherence.
2. Forward–backward IVR, whereby one approximates a double phase space integral by one (doubly long) single trajectory to account for forward and backward motion, including one extra integral over a jump parameter to account for a measurement of operator B; one complex phase of action is kept and averaged over (21, 23).
3. Full semiclassical dynamics, whereby one performs a full double phase space integral over all classical trajectories and keeps all complex phase factors. The most famous example is the Herman–Kluk (24, 25) approach with frozen Gaussians. Convergence can be difficult for long times and open systems.

In the context of nonadiabatic problems, this hierarchy is quite relevant because of the Meyer–Miller–Stock–Thoss (MMST) mapping (26–29). Consider a typical nonadiabatic problem (say, with N nuclei and two electronic states) expressed in a purely diabatic basis ($|L\rangle, |L'\rangle$). For such a problem, by replacing, e.g., $|L\rangle\langle L'| \rightarrow a_L^{\dagger} a_{L'}$, the MMST mapping transforms the nonadiabatic problem into an adiabatic problem with $N+2$ total degrees of freedom. Two of the resulting degrees of freedom are coupled harmonic oscillators, and this new basis is called the mapping basis. Thus, if one has a stable means to propagate adiabatic quantum dynamics, the MMST

mapping demonstrates how to propagate nonadiabatic quantum dynamics with only a marginal increase in computational cost.

Of course, as discussed above, the difficulty remains: propagating quantum dynamics exactly for big systems and long times is effectively impossible, and approximations must be made. Moreover, for nonadiabatic problems, the nuclear and electronic dynamics can be highly correlated. In applying the Miller semiclassical framework, one must be careful to balance the necessity for accuracy versus the practical need for convergence and numerical stability. Interestingly, if one applies the simplest LSC-IVR approximation to a nonadiabatic problem in the mapping basis, one finds that the resulting equations of motion are Ehrenfest (mean-field) dynamics (even though the initial conditions are different) (29–32). According to the Miller hierarchy, to go beyond mean-field dynamics, one must keep some phase information (which may or may not be stable for long times) (21).

2.3. Tully's Fewest Switches Surface Hopping Algorithm

To overcome the basic instabilities of exact quantum dynamical trajectories, Tully's (10) FSSH algorithm represents a totally different approach from the Miller semiclassical hierarchy. In seeking a meaningful and sufficiently accurate method to describe nonadiabatic dynamics efficiently, Tully chose not to start deductively from the Schrödinger equation. Instead, using intuition for how classical nuclei propagate both near and far away from electronic crossings, Tully proposed a set of rules for propagating trajectories and backing out dynamical information.

Let $|\Phi_j(\vec{R})\rangle$ and $|\Phi_k(\vec{R})\rangle$ be adiabatic states at position $\vec{R}$, and define

- V_{jj} as the potential energy surface for adiabat $|\Phi_j\rangle$, so that $\mathbf{H}_{\text{el}}(\vec{R})|\Phi_j(\vec{R})\rangle = V_{jj}(\vec{R})|\Phi_j(\vec{R})\rangle$;
- $\vec{F}_{jj}$ as the force acting on adiabat $|\Phi_j\rangle$, so that

$$\vec{F}_{jj}(\vec{R}) = -\left\langle \Phi_j(\vec{R}) \left| \frac{\partial \mathbf{H}_{\text{el}}}{\partial \vec{R}} \right| \Phi_j(\vec{R}) \right\rangle; \quad \text{and}$$

- $\vec{d}_{jk}$ as the derivative coupling between states $|\Phi_j\rangle$ and $|\Phi_k\rangle$, so that

$$\vec{d}_{jk}(\vec{R}) = \frac{\vec{F}_{jk}(\vec{R})}{V_{kk}(\vec{R}) - V_{jj}(\vec{R})}.$$

The Tully rules are as follows:

1. We assume that all dynamics start on a single adiabatic electronic state (but not a superposition). For example, for the case of photochemistry, we imagine starting 100% on the excited state ($|\Phi_2\rangle$) after photoexcitation.
2. We assume that, at time zero, we can sample the wavepacket's density with N_{traj} classical trajectories. Tully proposed propagating a handful of dynamical variables for each trajectory; see **Table 1**. In this framework, electronic amplitudes represent the electronic wavefunction of the system. If we start on the upper adiabatic state, the amplitudes for every trajectory are initialized as $\vec{c} = (0, 1)$ and the active surface is initialized as $\lambda = 2$.

Table 1 The four dynamical variables that Tully (10) chose to propagate in time assuming two electronic states

Variable	Description
$\vec{R}$	Array of nuclear positions
$\vec{P}$	Array of nuclear momenta
$\vec{c}$	Electronic amplitudes, $\vec{c} = (c_1, c_2)$
λ	Active adiabatic surface; can be 1 or 2

3. For every trajectory, the nuclei are propagated classically along the active surface λ:

$$\frac{\mathrm{d}\vec{R}}{\mathrm{d}t} = \frac{\vec{P}}{\vec{M}}, \tag{2}$$

$$\frac{\mathrm{d}\vec{P}}{\mathrm{d}t} = \vec{F}_{\lambda\lambda}. \tag{3}$$

4. One treats the electronic degrees of freedom completely quantum mechanically by integrating the electronic Schrödinger equation for the $\vec{c}$ amplitudes:

$$i\hbar\frac{\mathrm{d}c_j}{\mathrm{d}t} = V_{jj}(\vec{R})c_j - i\hbar\sum_{k\alpha}\frac{P^\alpha}{M^\alpha}d^\alpha_{jk}(\vec{R})c_k. \tag{4}$$

Sometimes it is convenient to propagate the electronic density matrix $\sigma_{ij} = c_i c_j^*$ instead of the amplitudes:

$$i\hbar\frac{\mathrm{d}\boldsymbol{\sigma}^{[j]}}{\mathrm{d}t} = \mathbf{V}(\vec{R})\boldsymbol{\sigma} - \boldsymbol{\sigma}\mathbf{V}(\vec{R}) - i\hbar\sum_{\alpha}\frac{P^\alpha}{M^\alpha}[\mathbf{d}^\alpha, \boldsymbol{\sigma}]. \tag{5}$$

5. At every time step, one calculates the probability to switch surfaces. For example, in the case of photochemistry, at early times before any switching has occurred, one calculates the probability of hopping downward from $|\Phi_2\rangle \rightarrow |\Phi_1\rangle$. The hopping rate from adiabatic surface j to adiabatic surface k is

$$\gamma_{\mathrm{tot}}^{j\rightarrow k} = \Gamma\left[\sum_\alpha \frac{2P^\alpha}{M^\alpha}\mathrm{Re}\left(d^\alpha_{jk}(\vec{R})\sigma_{kj}\right)\mathrm{d}t\right]\Big/\sigma_{jj}, \tag{6}$$

where $\mathrm{d}t$ is the simulation time step and Γ is the Heaviside function: $\Gamma[z] = z$ if $z > 0$, $\Gamma[z] = 0$ if $z < 0$.

The physical meaning underlying Equation 6 is the notion of FSSH. To explain this concept, suppose one has 60 trajectories on surface 2 and 40 trajectories on surface 1. Surface hopping assumes consistency between the $\vec{c}$ amplitudes and the active surfaces so that, if we ignore the differences between trajectories, we should expect that $\vec{c} = (\alpha, \beta)$, where $|\alpha|^2 = 0.4$ and $|\beta|^2 = 0.6$. Suppose further that, according to the electronic Schrödinger equation, after a time step $\mathrm{d}t$, the amplitudes become $\vec{c} = (\alpha', \beta')$, where $|\alpha'|^2 = 0.39$ and $|\beta'|^2 = 0.61$. In this case, consistency requires that we should now have 61 trajectories on surface 2 and 39 trajectories on surface 1. The essence of the FSSH scheme is that only one trajectory from surface 1 should hop up to surface 2. In other words, if we allowed two trajectories from surface 1 to hop up to surface 2 and one trajectory from surface 2 to hop down to surface 1, we would still obtain the desired result—but this would correspond to redundant hopping and would not accord with the FSSH ansatz.

6. When a hop occurs between active adiabatic surfaces (from $j \rightarrow k$), energy must be strictly conserved. Momenta are rescaled in the direction of the derivative coupling:

$$\vec{P}_{(j)} = \vec{P}_{(k)} + \Delta P \cdot \vec{d}_{jk}, \tag{7}$$

$$\vec{P}_{(j)} \cdot \frac{1}{2\vec{M}} \cdot \vec{P}_{(j)} + V_{jj}(\vec{R}) = \vec{P}_{(k)} \cdot \frac{1}{2\vec{M}} \cdot \vec{P}_{(k)} + V_{kk}(\vec{R}). \tag{8}$$

If a hop is not allowed energetically, the hop is called frustrated, and one ignores the hopping attempt. In such a case, one might attempt to reverse the velocity; see Section 6.3.

7. We assume that all physical quantities that must be calculated are either (*a*) exclusively nuclear operators (e.g., position, momentum, etc.) or (*b*) electronic operators that are

diagonal in the adiabatic representation. For example, to calculate the average position of a wavepacket, we average position coordinates over the swarm of trajectories (indexed by ζ):

$$\langle \vec{R} \rangle = \sum_{\zeta=1}^{N_{\text{traj}}} \frac{\vec{R}^{[\zeta]}}{N_{\text{traj}}}. \tag{9}$$

As another example, to calculate the average position for the wavepacket on adiabatic surface 2, we take the average position coordinate over the swarm

$$\langle \vec{R} \rangle_2 = \frac{\sum_{\zeta=1}^{N_{\text{traj}}} \vec{R}^{[\zeta]} \delta_{\lambda[\zeta]2}}{\sum_{\zeta=1}^{N_{\text{traj}}} \delta_{\lambda[\zeta]2}}. \tag{10}$$

These are the surface hopping rules (10) as prescribed by Tully and, on many occasions, these rules have been shown to give surprisingly accurate rates for electronic transitions and relaxation (33). [Note that the multiple-spawning algorithm of Martínez (8, 9) has also been very successful at modeling nonadiabatic dynamics. Multiple spawning can effectively be considered a more sophisticated version of surface hopping whereby independent trajectories are allowed to interact and transfer population; however, because trajectories always move along adiabatic surfaces, spawning achieves population transfer in a stable fashion.]

3. EARLY FRUSTRATIONS WITH AND CORRECTIONS FOR SURFACE HOPPING

Despite its successes, the FSSH model suffers from at least three problems.

3.1. Drawback 1: Decoherence

One problem with the FSSH algorithm is that it does not properly account for decoherence.

3.1.1. Identifying the phenomenon. It was only a few years after the FSSH algorithm was first proposed in 1990 that Rossky, Bittner, Schwartz & Prezhdo (34–37) recognized one crucial omission of surface hopping, namely the failure of the algorithm to properly account for decoherence. To explain this failure, consider the electronic density matrix

$$\boldsymbol{\sigma} = \begin{pmatrix} c_1 c_1^* & c_1 c_2^* \\ c_2 c_1^* & c_2 c_2^* \end{pmatrix}. \tag{11}$$

The off-diagonal matrix element σ_{12} should represent the overlap of a wavepacket on surface 1 with a wavepacket on surface 2. If these two wavepackets separate, one should find $\sigma_{12} \to 0$. However, FSSH does not necessarily feature this decay of the off-diagonal matrix element of $\boldsymbol{\sigma}$ (which is also called decoherence). When calculating the lifetime of a photoexcited, hydrated electron in water with the FSSH algorithm, Rossky and coworkers showed that, if the off-diagonal matrix element σ_{12} is not adjusted artificially, then the hopping rate of relaxation is too fast (see Equation 6). As a result, one finds erroneously short lifetimes (<100 fs) (36–39). Experimentally, one expects a population relaxation time of roughly 1 ps (36).

The phenomenon above can be illustrated easily with a simple example. In his original FSSH paper, Tully (10) himself observed the decoherence failures of the FSSH algorithm in the context of his third model problem, the so-called Extended Coupling Hamiltonian. Consider the one-dimensional potential energy surfaces shown schematically in **Figure 2** and a wavepacket entering the coupling region from the left along the lower surface. The two adiabatic surfaces are close in energy for $x < 0$ and will mix together near $x \approx -5$, near the peak of the derivative

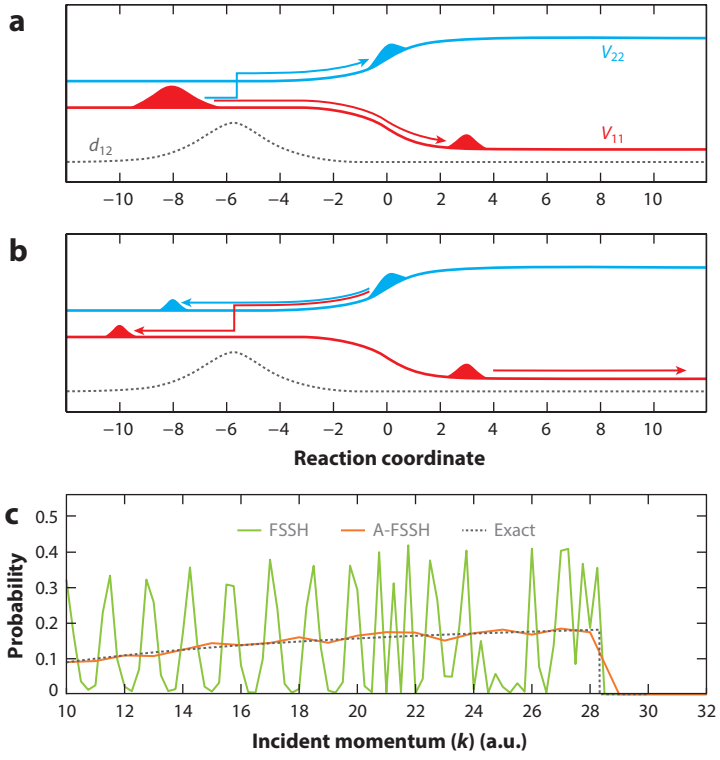

Figure 2

Decoherence and Tully's (10) third model problem. (*a*) Early times: The particle enters on the lower adiabatic surface V_{11} from the left and spawns a wavepacket on the upper surface V_{22} around $x \approx -5$, where the derivative coupling d_{12} peaks. (*b*) Later times: The lower wavepacket transmits and the upper wavepacket reflects, leading to a bifurcation. The upper wavepacket then goes back through the mixing region once more, this time spawning a wavepacket on the lower surface. (*c*) Probability of reflection on the lower surfaces as a function of incoming momentum (k). The standard fewest switches surface hopping (FSSH) algorithm predicts spurious oscillations because of the decoherence problem. An augmented fewest switches surface hopping (A-FSSH) (42, 43) algorithm with decoherence recovers the exact results by collapsing the amplitudes on the upper surface after reflection.

coupling. The incoming wavepacket on the lower surface will spawn into two wavepackets, and both of these wavepackets will continue moving together to the right.

Now, for $x > 0$, the upper adiabatic surface is repulsive, whereas the lower adiabatic surface leans forward. Thus, for low incoming velocity, the upper wavepacket will reflect backward and the lower wavepacket will transmit. There is no single moment of separation between these two wavepackets—rather, there is a rate of separation. As recognized by Rossky and coworkers, this rate of separation should be considered a decoherence rate, and is not included in the FSSH algorithm. [For the case of the photoexcited hydrated electron, this time scale is very fast—on the order of 3–6 fs (36–39).]

One can ask: What are the observable signatures of this FSSH failure? For scattering calculations, decoherence failures are observed only when a wavepacket moves through a mixing region (with large derivative coupling) more than one time (40, 41). In such a case, on the first crossing, the trajectory picks up an amplitude. On the second crossing, if the trajectory carries incorrect $\vec{c}$

amplitudes, the trajectory undergoes incorrect hops to incorrect surfaces, and the quality of the trajectory deteriorates rapidly. As a result, for the case of Tully's model problem 3, the FSSH branching ratios for reflection onto the upper and lower adiabatic states depend sensitively on the incoming velocity; the oscillations in **Figure 2*c*** are entirely spurious and reflect the incorrect decoherence behavior of the FSSH algorithm. Such oscillations may not be general, however; see Section 6.

3.1.2. Fixing up the algorithm. The obvious solution to the decoherence problem referenced above is to damp out the electronic amplitudes. If a trajectory is moving along active adiabatic surface 1, one wants to damp out the electronic amplitudes so that $(c_1, c_2) \rightarrow (1, 0)$. Such an operation should account for wavepacket bifurcation and should prevent artificial hops from arising. The only question is how one should operationally include such a decoherence time scale.

Several approaches have been proposed over the years:

- For sharp, isolated regions of mixing, the approach of Hammes-Schiffer and Fang (44, 45) is to simply monitor the strength of the derivative coupling along a given trajectory and then collapse the amplitudes when one leaves a region of large derivative coupling (and enters a region of small derivative coupling) according to some preset threshold parameter.
- Perhaps the most important insight into decoherence rates comes from the work of Rossky, Bittner, Schwartz & Prezhdo (36, 37), who imagined modeling a mother wavepacket and a recently spawned child wavepacket as two frozen Gaussians. On this basis, the decoherence rate $(1/\tau_d)$ must be proportional to the difference in forces,

$$1/\tau_d = \eta(F_{11} - F_{22}), \tag{12}$$

  but the question remains: What is the constant of proportionality η (with units 1/momentum)? Rossky and coworkers (36) used a thermal wavelength to estimate this constant and obtained an average (coarse-grained) decoherence time as a function of temperature in the condensed phase. Schwartz (46) has used this same rate of decoherence with Ehrenfest trajectories.
- More generally, it is desirable to construct a universal decoherence rate for both condensed-phase and gas-phase systems. In the context of the FSSH algorithm, Truhlar (47, 48) has repeatedly emphasized that the term "decoherence" connotes specifically the decay of the off-diagonal matrix element of the electronic subsystem; this decay can arise with just a single, gas-phase nuclear degree of freedom (just as in **Figure 2**). Thus, one would like to construct a decoherence rate that is independent of temperature (and, if possible, one without any other parameters). To that end, Jasper & Truhlar (49) proposed setting η in Equation 12 to be the inverse of the average momentum that can be evaluated in the gas phase; however, they also added another term to their decoherence rate (not proportional to $\Delta\vec{F}$). As discussed in the Appendix, there is an interesting history regarding the differences between the rates proposed by Rossky and Truhlar.
- One final approach to decoherence was made by Prezhdo & Rossky (50), who suggested running FSSH and Ehrenfest dynamics simultaneously. By comparing the differences between these two methods, the authors attempted to estimate the overcoherence errors of FSSH and to capture a decoherence rate for FSSH (but the exact rate required some parameterization). In practice, the method was usually augmented with some additional, empirical decoherence (38, 39).

Thus, historically, the first drawback of the FSSH algorithm has been the lack of a rigorous approach for calculating a decoherence rate without any parameterization that works for both condensed-phase and gas-phase problems.

3.2. Drawback 2: Initial Conditions and Diabatic Populations

Although Tully (10) originally argued that FSSH could be run in either a diabatic or an adiabatic basis, in practice the algorithm is almost always run in an adiabatic basis (with good reason; see Section 4.1; see also Reference 51.) This basis dependence inevitably raises the question of how one should calculate diabatic populations. A related question is how one defines the initial conditions if the system is not restricted to a single adiabatic state at time $t = 0$. Consider, for example, the state of a molecule after excitation with a photon. After one interaction with a photon field, the electronic state of the system is $|\Psi\rangle = c_1|\Phi_1\rangle + c_2|\Phi_2\rangle$. How do we run dynamics corresponding to these initial conditions (now that we are starting in a coherent superposition of adiabatic states rather than in one adiabatic state)?

In fact, this question of initialization arises in many other cases as well. For instance, suppose we are interested in photoexcited dynamics and we are prepared to approximate that the dynamics should be initialized on a diabatic state $|\Xi_a\rangle$. What do we do if the excited state $|\Xi_a\rangle$ is actually mixed with another excited state, e.g., $|\Xi_b\rangle$? In such a case, there are two adiabatic states, $|\Phi_1\rangle$ and $|\Phi_2\rangle$, each with a nonzero projection onto state $|\Xi_a\rangle$:

$$\begin{pmatrix}|\Phi_1\rangle\\|\Phi_2\rangle\end{pmatrix} = \begin{pmatrix}\cos\theta & \sin\theta\\ -\sin\theta & \cos\theta\end{pmatrix}\begin{pmatrix}|\Xi_a\rangle\\|\Xi_b\rangle\end{pmatrix} \iff \begin{pmatrix}|\Xi_a\rangle\\|\Xi_b\rangle\end{pmatrix} = \begin{pmatrix}\cos\theta & -\sin\theta\\ \sin\theta & \cos\theta\end{pmatrix}\begin{pmatrix}|\Phi_1\rangle\\|\Phi_2\rangle\end{pmatrix}. \quad (13)$$

Again, the question arises of what the appropriate means is to initialize dynamics. Presumably we must initialize dynamics stochastically on the different adiabatic surfaces—but how do we initialize the amplitudes? For a trajectory that starts on adiabat 1, is it best to initialize the amplitudes as

$$\begin{pmatrix}c_1\\c_2\end{pmatrix} = \begin{pmatrix}1\\0\end{pmatrix}, \quad (14)$$

or is

$$\begin{pmatrix}c_1\\c_2\end{pmatrix} = \begin{pmatrix}\cos\theta\\-\sin\theta\end{pmatrix} \quad (15)$$

better?

A related source of confusion for the surface hopping algorithm, and one with a long history, is the question of computing diabatic populations. Suppose that we are running dynamics for a swarm of excited-state surface hopping trajectories, which are propagating along adiabatic surfaces $|\Phi_1\rangle, |\Phi_2\rangle$. Often, one would like to compute the probability D_a of populating diabatic state $|\Xi_a\rangle$. This question has been asked by many researchers in the past (52–57). Traditionally, there have been two approaches, neither of them completely successful. On the one hand, one can use the amplitudes ($\vec{c}$) exclusively (52, 53) and average over all N_{traj} trajectories. Thus,

$$D_a^{\text{amp}} \equiv \sum_{\zeta=1}^{N_{\text{traj}}} \frac{1}{N_{\text{traj}}}\left(c_1^{[\zeta]}\cos\left(\theta(\vec{R}^{[\zeta]})\right) - c_2^{[\zeta]}\sin\left(\theta(\vec{R}^{[\zeta]})\right)\right)^2. \quad (16)$$

On the other hand, one can use the surfaces (λ) exclusively (54–57). In this case,

$$D_a^{\text{surf}} \equiv \sum_{\zeta=1}^{N_{\text{traj}}} \frac{1}{N_{\text{traj}}}\left(\delta_{\lambda[\zeta]1}\cos^2\left(\theta(\vec{R}^{[\zeta]})\right) + \delta_{\lambda[\zeta]2}\sin^2\left(\theta(\vec{R}^{[\zeta]})\right)\right). \quad (17)$$

Neither of these two approaches is satisfactory.

- Using amplitudes alone (Equation 16), one finds accurate answers at short times but meaningless answers at long times. For instance, at long times, the amplitudes do not recover detailed balance at all (58, 59).

- Vice versa, using the surfaces to convert to a diabatic basis (Equation 17), one does recover detailed balance at long times (58, 59), but the answer is usually incorrect at short times (60). For instance, suppose a calculation must begin on diabat $|\Xi_a\rangle$. As discussed above, because FSSH propagates trajectories along adiabats, one is forced to convert to the adiabatic basis ($|\Phi_1\rangle$, $|\Phi_2\rangle$). Now, suppose we have converted to an adiabatic basis and want to measure the population D_a of diabat a immediately thereafter (say, after 0.1 fs). If we measure diabatic populations with only the surface data (as in Equation 17), we may well find $D_a \ll 1$ (which is completely unphysical); see **Figure 5**.

In short, the second historical drawback of the FSSH algorithm is that, until recently, there was no universally reliable method for computing diabatic populations. Different practitioners have used different definitions for different purposes: One should use amplitudes for short times and surfaces for long times.

3.3. Drawback 3: Quantum Classical Liouville Equation

In 1990, the FSSH algorithm was postulated by Tully as an ansatz, but the algorithm was never derived from the Schrödinger equation. Thus, the algorithm has often been considered ad hoc (61, 62), and the reliability of FSSH results has been questioned. In the late 1990s, there was a rush of activity to develop a rigorous framework for deriving a surface hopping methodology (63–66). This activity was centered around the quantum classical Liouville equation (QCLE) (63–72). The premise of the QCLE is to perform a Wigner transformation over the nuclear coordinates only:

$$A_{ij}^{\mathrm{W}}(\vec{R},\vec{P},t) \equiv \left(\frac{1}{2\pi\hbar}\right)^{3N} \int \mathrm{d}\vec{X}\, e^{i\vec{P}\cdot\vec{X}/\hbar} \left\langle \Phi_i(\vec{R});\vec{R}-\frac{\vec{X}}{2}\right| \Psi(t)\rangle\langle \Psi(t) \left|\Phi_j(\vec{R});\vec{R}+\frac{\vec{X}}{2}\right\rangle. \quad (18)$$

Here, $|\Phi_i(\vec{R})\rangle$, $|\Phi_j(\vec{R})\rangle$ are the adiabatic electronic eigenstates at position $\vec{R}$. $|\Psi(t)\rangle$ represents the full, nuclear electronic wavefunction at time t.

The definition in Equation 18 may look slightly intimidating, but it is in fact quite simple. As an example, in **Figure 3**, we plot the A_{ij}^{W} densities for the exact nuclear electronic wavefunction that is propagated along the Hamiltonian for Tully's model problem 3. We focus on just that moment in time when the wavepacket on the upper surface is pulling away from the wavepacket on the lower surface (see **Figure 2*a***). In **Figure 3**, A_{11}^{W} is the Wigner transform for the wavepacket on the lower surface, A_{22}^{W} is the Wigner transform for the wavepacket on the upper surface, and A_{12}^{W} is the Wigner transform for the wavepacket on the 1–2 coherence.

Now, to connect Equation 18 with a surface hopping algorithm, one can calculate an approximate mixed quantum–classical equation of motion (EOM) for the partial Wigner transform. This EOM can be obtained by cutting off all terms linear or higher in $\hbar$ or, equivalently, by making a mass expansion (63–66). Alternatively, the same EOM can be derived by propagating a mixed nuclear–electronic density matrix with path integrals and linearizing all path integrals for the nuclei only (74). The resulting equation is the QCLE:

$$\begin{aligned}\frac{\partial}{\partial t}A_{ij}^{\mathrm{W}}(\vec{R},\vec{P},t) = {} & \frac{-i}{\hbar}\Big(V_{ii}(\vec{R})-V_{jj}(\vec{R})\Big)A_{ij}^{\mathrm{W}} \\ & -\sum_{\alpha}\frac{P^{\alpha}}{M^{\alpha}}\sum_{k}\Big(d_{ik}^{\alpha}(\vec{R})A_{kj}^{\mathrm{W}}-A_{ik}^{\mathrm{W}}d_{kj}^{\alpha}(\vec{R})\Big)-\sum_{\alpha}\frac{P^{\alpha}}{M^{\alpha}}\frac{\partial A_{ij}^{\mathrm{W}}}{\partial R^{\alpha}} \\ & -\frac{1}{2}\sum_{k\alpha}\left(F_{ik}^{\alpha}(\vec{R})\frac{\partial A_{kj}^{\mathrm{W}}}{\partial P^{\alpha}}+\frac{\partial A_{ik}^{\mathrm{W}}}{\partial P^{\alpha}}F_{kj}^{\alpha}(\vec{R})\right).\end{aligned} \quad (19)$$

The QCLE is exact for the spin-boson model Hamiltonian.

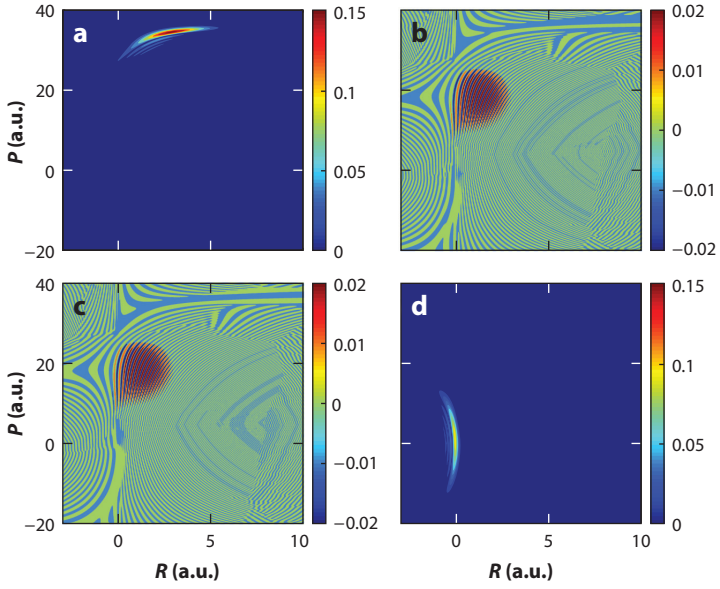

Figure 3

The partial Wigner transform of the exact wavefunction for a particle scattering through Tully's (10) third model problem, near the time when the two wavepackets begin to separate. For the wavepacket cartoon in real space, see **Figure 2*a***. (*a*) $A_{11}^{W}(R, P)$; (*b*) Re $\left(A_{12}^{W}(R, P)\right)$; (*c*) Im $\left(A_{12}^{W}(R, P)\right)$; (*d*) $A_{22}^{W}(R, P)$. The lower wavepacket on $|\Phi_1\rangle$ is centered near $(R, P) = (3, 30)$ and is transmitting. The upper wavepacket on $|\Phi_2\rangle$ is centered near $(R, P) = (0, 0)$ and is about to reflect. The coherence density is centered in between and is highly oscillatory. For more details, see Reference 73.

Kapral and coworkers (65, 66) have shown that Equation 19 can be approximated well in terms of a surface hopping–like algorithm in the adiabatic basis, with momentum jumps in the direction of the derivative couplings. However, Kapral's momentum-jump algorithm is unlike Tully's algorithm. Whereas Tully's surface hopping algorithm requires hops between adiabatic surfaces, the Kapral momentum-jump algorithm requires not only jumps between adiabatic surfaces but also jumps between adiabatic surfaces and coherence surfaces. If $V_{11}(R)$ and $V_{22}(R)$ denote adiabatic surfaces 1 and 2, then the 1–2 coherence is associated with potential energy $(V_{11}(R) + V_{22}(R))/2$ (75–79). Unfortunately, this momentum-jump scheme is numerically unstable, effectively because some trajectories acquire a negative weighting.

Historically, the third drawback of the FSSH algorithm has been the absence of any concrete relationship between Tully's surface hopping approach and Kapral's momentum-jump algorithm. After all, the QCLE can be related directly to the Schrödinger equation, so one must wonder: If the FSSH algorithm is a legitimate scheme, what is the exact relationship between the FSSH algorithm and the QCLE (Equation 19)?

4. THEORY: RECENT ADVANCES

In recent years, there has been a surge of activity in the arena of surface hopping and, for the most part, the three central questions above have been answered.

4.1. A Quasi-Derivation of the Fewest Switches Surface Hopping Algorithm from the Quantum Classical Liouville Equation in the Adiabatic Basis (Response to Drawback 3)

The most important development concerning surface hopping has been the explicit connection between Tully's algorithm and the QCLE. In Reference 80, our group showed that—under a host of assumptions, some of which are discussed below—the FSSH algorithm in the adiabatic basis can be approximately derived from the QCLE. The most important of these assumptions are the following three:

1. We assume that the wavepacket has a large velocity in the direction of the derivative coupling, so that total momentum is much larger than the momentum rescaling difference, $P \gg \Delta P$. This allows us to neglect frustrated hops.
2. Considering the swarm of particles, we assume that, at any given time t, there is a single, unique trajectory at any given point in phase space $(\vec{R}, \vec{P})$ moving along surface λ. Thus, there is a unique electronic density matrix for such a point in phase space $\boldsymbol{\sigma}^{(\lambda)}(\vec{R}, \vec{P}, t)$.
3. The electronic Schrödinger equation above (Equation 5) must be adjusted, in part so as to account for decoherence.

With these assumptions, the FSSH algorithm can be connected to the QCLE, which puts the FSSH algorithm on firmer formal ground. The key object to define is the nuclear–electronic density matrix for a swarm of FSSH trajectories, $A_{ij}^{\mathrm{FSSH}}(\vec{R}, \vec{P}, t)$. The on-diagonal density matrix elements can be defined as follows (using only the active surface information, not the amplitudes):

$$A_{11}^{\mathrm{FSSH}}(\vec{R}, \vec{P}, t) \equiv \lim_{N_{\mathrm{traj}}\to\infty} \frac{1}{N_{\mathrm{traj}}} \sum_{\zeta=1}^{N_{\mathrm{traj}}} \sum_{\lambda_0=1}^{2} \int \mathrm{d}\vec{R}_0 \int \mathrm{d}\vec{P}_0 \; A_{\lambda_0\lambda_0}^{\mathrm{W}}(\vec{R}_0, \vec{P}_0)\, \delta\Big(\vec{R}_t(\vec{R}_0, \vec{P}_0, \lambda_0, \zeta) - \vec{R}\Big) \times \delta\Big(\vec{P}_t(\vec{R}_0, \vec{P}_0, \lambda_0, \zeta) - \vec{P}\Big)\delta_{\lambda(t),1}. \tag{20}$$

A_{22}^{FSSH} is defined analogously.

Equation 20 can be understood easily on physical grounds. $\vec{R}_0$, $\vec{P}_0$, and λ_0 label the initial position, momentum, and active surface for a given trajectory at time 0; ζ represents a random number generating seed for the stochastic dynamics. For surface 1, the phase space density $A_{11}^{\mathrm{FSSH}}(\vec{R}, \vec{P}, t)$ is just the density of trajectories with active surface 1 sitting in phase space at $(\vec{R}, \vec{P})$ at time t. $A_{22}^{\mathrm{FSSH}}(\vec{R}, \vec{P}, t)$ is defined similarly for surface 2. According to Equation 20, the trajectories should be initiated starting from the true, partially Wignerized density matrix at time $t = 0$ [so that $A_{11}^{\mathrm{FSSH}}(\vec{R}, \vec{P}, 0) = A_{11}^{\mathrm{W}}(\vec{R}, \vec{P}, 0)$]. Here, we already see one condition for the validity of surface hopping: We assume that, at time 0, $A_{11}^{\mathrm{W}}(\vec{R}, \vec{P}, 0)$ and $A_{22}^{\mathrm{W}}(\vec{R}, \vec{P}, 0)$ are both strictly positive, which is effectively a high-temperature ansatz (which is consistent with Assumption 1 above).

To construct the off-diagonal matrix elements, one must use the $\vec{c}$ amplitudes or, more conveniently, the $\boldsymbol{\sigma}$ electronic density matrix. Here, there are two possible (and incompatible) definitions. If the active surface is $\lambda = 1$, it is convenient to consider

$$A_{12}^{(1)}(\vec{R}, \vec{P}, t) \equiv \frac{\sigma_{12}^{(1)}(\vec{R}, \vec{P}, t)}{\sigma_{11}^{(1)}(\vec{R}, \vec{P}, t)} A_{11}^{\mathrm{FSSH}}(\vec{R}, \vec{P}, t). \tag{21}$$

If the active surface is $\lambda = 2$, however, it is convenient to consider

$$A_{12}^{(2)}(\vec{R}, \vec{P}, t) \equiv \frac{\sigma_{12}^{(2)}(\vec{R}, \vec{P}, t)}{\sigma_{22}^{(2)}(\vec{R}, \vec{P}, t)} A_{22}^{\mathrm{FSSH}}(\vec{R}, \vec{P}, t). \tag{22}$$

Here, we invoke the unique trajectory assumption above (Assumption 2), so that at point (R, P) at time t, there is only one unique trajectory on surface λ with electronic density matrix $\boldsymbol{\sigma}^{(\lambda)}$.

Using the definitions in Equations 21 and 22 and making Assumptions 1 and 2, one can show [after some very tedious algebra (80)] that, when propagated in the adiabatic basis, the FSSH density matrix A_{ij}^{FSSH} almost satisfies the QCLE. For agreement with the QCLE, however, the EOM for the electronic density matrix (Equation 5) must be adjusted. If $\lambda = 1$ is the active surface, these equations must be altered to read:

$$\frac{\mathrm{d}}{\mathrm{d}t}\sigma_{12}^{(1)} = \frac{-i}{\hbar}\left(V_{11} - V_{22}\right)\sigma_{12}^{(1)} - \sum_{\alpha} d_{12}^{\alpha}\left(\sigma_{22}^{(1)} - \sigma_{11}^{(1)}\right)\frac{P^{\alpha}}{M^{\alpha}} - \gamma_{12}^{(1)}\sigma_{12}^{(1)}, \tag{23}$$

$$\frac{\mathrm{d}}{\mathrm{d}t}\sigma_{22}^{(1)} = -\sum_{\alpha}\frac{P^{\alpha}}{M^{\alpha}}\left(d_{21}^{\alpha}\sigma_{12}^{(1)} - \sigma_{21}^{(1)}d_{12}^{\alpha}\right) - \gamma_{22}^{(1)}\sigma_{22}^{(1)}. \tag{24}$$

The exact form for $\gamma_{12}^{(1)}$ and $\gamma_{22}^{(1)}$ in Equations 23 and 24 can be found in Reference 80. The dominant contributions, however, are simple:

$$\gamma_{12}^{(1)} \approx \frac{1}{2}\sum_{\alpha}\left(F_{22}^{\alpha} - F_{11}^{\alpha}\right)\frac{1}{A_{12}^{(1)}}\frac{\partial A_{12}^{(1)}}{\partial P^{\alpha}}, \tag{25}$$

$$\gamma_{22}^{(1)} \approx \sum_{\alpha}\left(F_{22}^{\alpha} - F_{11}^{\alpha}\right)\frac{1}{A_{22}^{\mathrm{FSSH}}}\frac{\partial A_{22}^{\mathrm{FSSH}}}{\partial P^{\alpha}}. \tag{26}$$

Equations 23–26 constitute Assumption 3 above and are statements about decoherence. Just as was predicted by Rossky and coworkers, we now see that the off-diagonal matrix elements (as well as the population on the inactive surface) should be damped by a factor η (see Equation 12) multiplied by the difference in adiabatic forces.

4.2. Decoherence and Recoherence Revisited with Augmented Fewest Switches Surface Hopping (Response to Drawback 1)

We are now in a position to address decoherence and recoherence in the context of the FSSH algorithm.

4.2.1. Decoherence. With regard to decoherence, the prefactors in Equations 25 and 26, corresponding to η in Equation 12, are very illuminating. Clearly, the exact decoherence rate requires knowledge of the local derivatives of the density of the Wigner representation, e.g., $(1/A_{12}^{(1)})(\partial A_{12}^{(1)}/\partial P^{\alpha})$. Thus, for an exact decoherence rate, all trajectories would need to be propagated together and every trajectory would need to know the location in phase space (and the electronic state) of every other trajectory. Noninteracting trajectories are insufficient for exact dynamics.

At this point, one would appear to be stuck. On the one hand, dynamics with interacting trajectories are almost always unstable, especially in high-dimensional systems; see the discussion of Bohmian mechanics in Section 2.1. On the other hand, the FSSH algorithm needs a decoherence rate and, with its very limited number of variables (see **Table 1**), it is not clear how to even estimate such a rate. Thus, in practice, one might be tempted to simply ignore all decoherence effects (and use standard FSSH) or use a heuristic, parameterized version of decoherence (perhaps as a function of temperature).

Faced with this dire situation, our research group has proposed a solution in between these two extremes: augmenting the standard FSSH algorithm (42, 43) so that, beyond the variables in **Table 1**, each independent trajectory carries two more variable arrays that can be used explicitly for the purpose of estimating decoherence rates. These additional variables are the position and momentum moments (81–84) of the total nuclear–electron wavefunction $|\Psi\rangle$ as projected onto

Table 2 The extra dynamical variables (in addition to those in Table 1) that are propagated by augmented FSSH (42, 43)

Variable	Description
$\Delta\vec{R}_{ii}$	Position moments for nuclear wavepacket moving along adiabat $\|\Phi_i\rangle$
$\Delta\vec{P}_{ii}$	Momentum moments for nuclear wavepacket moving along adiabat $\|\Phi_i\rangle$
$\Delta\vec{R}_{ij}$	Position moments for nuclear wavepacket for ij coherence
$\Delta\vec{P}_{ij}$	Momentum moments for nuclear wavepacket for ij coherence

each adiabatic state; see **Table 2**. The moments in **Table 2** are the most obvious and most natural variables for each trajectory to carry along. These moments can be propagated (approximately) along any given trajectory and, if one continuously integrates the difference in forces $\Delta\vec{F} = \vec{F}_{11} - \vec{F}_{22}$, they capture some part of wavepacket bifurcation. With a few approximations and a few assumptions, and assuming one is moving along active adiabatic surface 1, one can estimate a lower bound for the decoherence rate:

$$\frac{1}{\tau_d} \approx \sum_{\alpha} \left(\frac{(F^{\alpha}_{22} - F^{\alpha}_{11})\left(\Delta R^{\alpha}_{22}\right)}{2\hbar} \right). \tag{27}$$

For all definitions and EOMs (and a few more details), see References 42 and 43. If the $\vec{c}$ amplitudes are damped (or collapsed) with the rate defined in Equation 27, we call the resulting algorithm augmented FSSH (A-FSSH). To date, we have found that almost all surface hopping calculations are improved by including this decoherence (but see below for the recoherence exception to this rule).

4.2.2. Recoherence. The quasi-derivation in Section 4.1 makes clear that there are two different notions of recoherence for FSSH calculations. The first notion of recoherence is depicted in **Figure 4*a***. Here, one imagines two separated wavepackets meeting at a region with derivative coupling, leading to population transfer and interference (85). As an extreme example, these two wavepackets could finally recombine into one wavepacket on one surface, as in **Figure 4*a***. In this case, the FSSH algorithm is not able to recover the correct interference signal, which follows directly from the unique trajectory assumption above (Assumption 2).[1]

As depicted in **Figure 4*b***, the second notion of recoherence is slightly more feasible for surface hopping calculations. Here, one imagines monitoring the overlap of two wavepackets moving along different surfaces, but one assumes that there is no avoided crossing between them (i.e., no population decay). This state of affairs would correspond to the case of pure dephasing in spectroscopy, where one seeks to evaluate the time dependent overlap, and one expects to find that the overlap should wax and wane. With this in mind, it is useful to reconsider Equations 25 and 26. Notice that the γ's can in fact be either positive or negative. Thus, in principle, in order for the FSSH algorithm to match the QCLE, we should sometimes damp the coherence between adiabats 1 and 2 (as if the two wavepackets were moving apart, or decohering), and we should sometimes grow the coherence between adiabats 1 and 2 (as if the two wavepackets were

[1]Note that, in the case of Tully's (10) problem 2, all scattering calculations are performed at constant energy, so the effects of such recoherences are minimal. For this model problem, in fact, the surfaces are similar enough that one can recover the correct Stückelberg oscillations approximately at high energy by integrating the electronic Schrödinger equation in time while assuming that the nuclei continue forward (in the spirit of the classical path approximation) without any feedback.

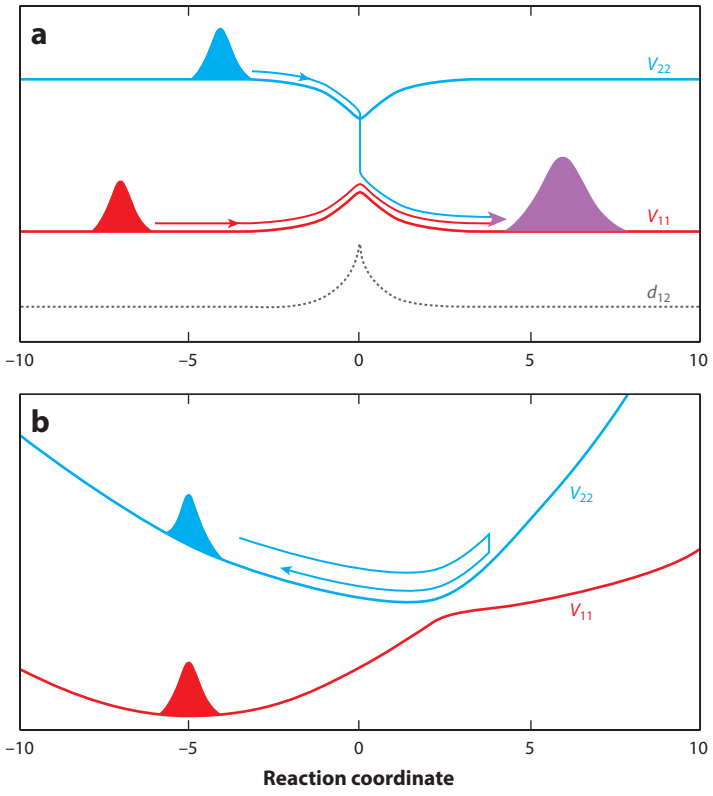

Figure 4

Two forms of recoherences. (*a*) Separated wavepackets from different surfaces recombining as mediated through a derivative coupling. These interferences cannot be captured by any form of surface hopping. (*b*) The overlaps between wavepackets on different surfaces can oscillate as the wavepackets eventually dephase. We refer to those periods of time, during which the overlaps are growing, as recoherences; these features are ignored if we apply a decoherence correction. Here, the potential energy surfaces are labeled V_{11} and V_{22} and the derivative coupling is d_{12}.

coming together, or recohering). In practice, however, to our knowledge, no one has ever tried to grow the coherence matrix element; in general, because these coherences are very short-lived (especially in high-dimensional systems), most of the effort in surface hopping development is to recover decoherence correctly without worrying about recoherence. In other words, one considers wavepacket bifurcation to be completely irreversible.

That being said, there is reason to worry about the ability of A-FSSH (or any decoherence correction, for that matter) to recover gas-phase electronic spectra with vibronic structure. Indeed, we have found (86–88) that A-FSSH spectra for gas-phase molecules can be far too broad. In such a case, FSSH [or, in fact, Ehrenfest dynamics (88)] is a better approach. In condensed-phase systems, however, with moderate to strong coupling to the environment, we almost always find that including decoherence alone (and ignoring recoherence) improves the quality of a simulation.

4.3. Changing Electronic Basis (Response to Drawback 2)

Lastly, regarding the questions of initialization and diabatic populations, the quasi-derivation in Section 4.1 provides all necessary solutions. First, for choosing initial conditions, clearly

Equation 15 is correct and Equation 14 is incorrect. Second, for calculating diabatic populations (or, for that matter, any electronic observable), the formalism in Section 4.1 provides a unique answer. Whereas both approaches discussed in Section 3.2, one based on amplitudes and one based on surfaces, are incorrect, we now find a third methodology that is optimal. According to this third option, we use both surface and amplitude information to build the correct density matrix for the FSSH algorithm. According to this density matrix option, the population on diabat a is then specified as

$$D_a^{\text{dens}} = \sum_{\zeta=1}^{N_{\text{traj}}} \frac{1}{N_{\text{traj}}} \left(\delta_{\lambda[\zeta]1} \cos^2\left(\theta(\vec{R}^{[\zeta]})\right) + \delta_{\lambda[\zeta]2} \sin^2\left(\theta(\vec{R}^{[\zeta]})\right) - 2c_1^{[\zeta]} c_2^{[\zeta]} \sin\left(\theta(\vec{R}^{[\zeta]})\right) \cos\left(\theta(\vec{R}^{[\zeta]})\right) \right). \tag{28}$$

The density matrix prescription in Equation 28 captures the best parts and avoids the worst parts of Equations 16 and 17. On the one hand, because of the presumed consistency between surfaces and amplitudes at short times, Equations 28 and 16 should be identical at short times. Thus, the density matrix option recovers the correct transient dynamics experienced by the electrons as predicted by the amplitude option, before the nuclei move around too much and initiate relaxation. On the other hand, at long times, one can expect that different trajectories will carry different phases in their $\vec{c}$ amplitudes, and thus any average should go to zero:

$$\sum_{\zeta=1}^{N_{\text{traj}}} \frac{2c_I^{[\zeta]} c_J^{[\zeta]} \sin\left(\theta(\vec{R}^{[\zeta]})\right) \cos\left(\theta(\vec{R}^{[\zeta]})\right)}{N_{\text{traj}}} \to 0. \tag{29}$$

Thus, one can safely expect that, at long times, Equations 28 and 17 are identical. Moreover, because the number of trajectories on each adiabat should approximately obey detailed balance (58, 59), at long times, the populations according to the density matrix option should also satisfy detailed balance approximately.

5. KEY COMPUTATIONAL RESULTS

5.1. Spin-Boson Model Hamiltonian

The spin-boson Hamiltonian is the simplest model problem for studying nonadiabatic effects in the condensed phase. One considers a two-level system (corresponding to an electronic degree of freedom) coupled linearly to a bath of bosons (corresponding to many nuclear degrees of freedom). The two levels are also coupled directly through the diabatic coupling, V_c. Although the spin-boson model cannot be solved analytically, there has been great progress over the last twenty years in developing exact methods to solve for the dynamics of the electronic subsystem. As developed by Makri and coworkers in the early 1990s (17, 18), a quasi-adiabatic path integral (QUAPI) allows one to solve a certain class of spin-boson model problems exactly, whenever the memory kernel decays fast enough; within this constraint, the spectral density can be chosen arbitrarily. More recently, Tanimura (19, 89) and Ishizaki (90) pioneered the hierarchial equations of motion (HEOM) that allow one to propagate the electronic density matrix for a much broader range of Hamiltonians. In practice, as long as the spectral density is chosen to be of Debye form (or some linear combination thereof), the HEOM protocol can correctly interpolate all the way from the nonadiabatic Marcus regime (small diabatic couplings and relatively large system–bath couplings) to the Redfield regime (small system–bath couplings and relatively large diabatic couplings). When converged, QUAPI and HEOM represent exact dynamics against which we can benchmark approximate dynamical schemes, including surface hopping.

5.1.1. Scaling of the rate for the nonadiabatic Marcus regime: effect of decoherence. The nonadiabatic regime of the spin-boson model (with small diabatic coupling V_c) has long been studied through the lens of stochastic trajectories (91, 92). Partial benchmarks of the FSSH algorithm for the spin-boson problem were performed by Landry & Subotnik (43, 56), Schwerdtfeger & Hammes-Schiffer (55), Jain & Subotnik (93), Ben-Nun & Martínez (94), and Chen & Reichman (95).

One important result is that the standard FSSH algorithm does not recover the correct scaling for the relaxation. According to Marcus theory, for the standard spin-boson problem with small diabatic coupling V_c and at classical temperatures, the rate of relaxation from diabat a to diabat b is

$$k_{\text{Marcus}} = \frac{V_c^2}{\hbar}\sqrt{\frac{\pi}{E_r k_B T}}\exp^{-\Delta G^{\ddagger}}. \tag{30}$$

Here, E_r is the reorganization energy and $\Delta G^{\ddagger}$ is the barrier height. Like any other Fermi's golden rule rate, Equation 30 scales as V_c^2. References 56 and 96 show, however, that the FSSH algorithm sometimes predicts scaling that is linear in V_c (rather than V_c^2) if the driving force is large enough. This failure of the FSSH algorithm can be traced to the fact that if V_c is small and if friction is not too large, the system goes through the crossing many times before it relaxes into a different well. Thus, the decoherence failures of the FSSH algorithm are amplified dramatically in the nonadiabatic regime.

With this failure in mind, Jain, Landry & Subotnik (43, 93) have recently demonstrated that, provided that the temperature is large enough that the nuclei can be treated classically and decoherence is included correctly, the A-FSSH algorithm does describe relaxation (both short-time transients and long-time rates) well. In particular, A-FSSH does agree with Marcus theory where appropriate (93, 95); see Section 6.3.

5.1.2. Diabatic populations with reasonably large diabatic couplings. When the diabatic coupling is reasonably large, the two historical schemes for calculating diabatic populations (see Section 3.2) are both incorrect, and the correct scheme for calculating diabatic populations (see Section 4.3) performs best. In **Figure 5**, we plot the donor diabatic population (which equals 1 initially) for the case $V_c = E_r$. The donor diabat has a higher energy than the acceptor diabat, and the donor population decays in time. Observe that, at short times, the diabatic populations calculated with the FSSH amplitudes look good; but these populations become meaningless at long times. Vice versa, observe that, at long times, the diabatic populations calculated from the FSSH surfaces look good; but they make no sense at short times. Finally, observe that the diabatic populations calculated from the FSSH density matrix look the best of all, interpolating from the amplitude data (at short times) to the surface data (at long times).

5.2. Applications to Electron and Energy Transfer

Finally, perhaps the most important function of the surface hopping algorithm is the ease with which the algorithm allows us to propagate nonadiabatic dynamics for large systems. This convenience has allowed a great deal of exploration in theoretical chemistry, whereby one can gain intuition about excited molecules without necessarily needing to run massive and expensive calculations. For instance, Yarkony & Zhu (97) recently used the FSSH algorithm to sample the configuration space of phenol in search of the important crossing regions. After running the FSSH algorithm and gathering the relevant data set, Yarkony & Zhu constructed global diabatic potential energy surfaces for three states.

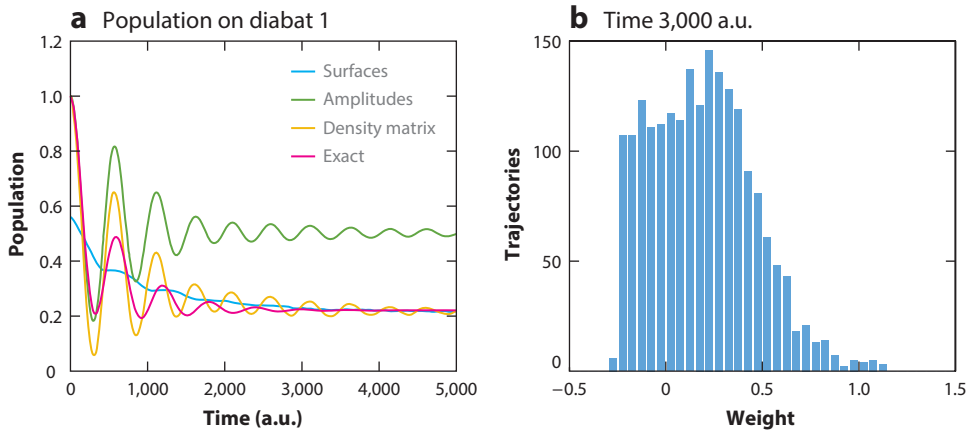

Figure 5

(*a*) Diabatic populations for the spin-boson model as computed with (*blue line*) surfaces only (Equation 17), (*green line*) amplitudes only (Equation 16), and (*yellow line*) the density matrix (Equation 28) for the case $V_c = E_r$. Note that only the density matrix approach recovers the correct short- and long-time behavior. (*b*) A histogram of all N_{traj} contributions to the average in Equation 28. We do find some negative terms averaged together for the population, but the final average is always found (empirically) to be positive, and convergence is rapid. Here, we use 2,000 trajectories for both left and right panels. The exact parameters for this model Hamiltonian can be found in figure 1 in Reference 60.

Beyond the exploration of potential energy surfaces, some of the most interesting applications of the FSSH algorithm have been in the area of organic photovoltaics and energy transfer. In this arena, Rossky and coworkers (98) and Tretiak and coworkers (99) have shown that, using semi-empirical excited state methodologies, one can model large conjugated polymers over long time scales. In the course of their simulations, one can observe (*a*) how energy transfer is propagated and what motions lead to energy transfer and (*b*) the length of electronic delocalization as excitons propagate. Thus, the surface hopping algorithm has allowed some theoretical insight into the complicated nature of organic electronics, which is becoming a popular area of research.

Lastly, regarding ab initio calculations, Barbatti, Lishcka and coworkers (13, 100–102) have created the Newton-X program to run the FSSH algorithm with electronic structure on the fly, usually at the level of time-dependent density functional theory (TD-DFT) or multiconfigurational self-consistent field theory. [Note that derivative couplings for TD-DFT excited states are now available commercially (103–109, 112–114).] These authors have performed photochemical calculations of small organic chromophores that have yielded insight into the mechanisms of bond-making and -breaking in the excited state. Recently, Landry & Subotnik (3) reported the first ab initio FSSH dynamical studies of energy transfer for a donor–bridge–acceptor molecule [albeit at a low level of electronic structure theory (configuration interaction singles)], as shown in **Figure 1**. A-FSSH is now available in Q-Chem (115).

In sum, the overwhelming strength of the FSSH approach is the ability to do exploratory calculations of excited state dynamics in new systems with a minimum of overhead. To date, the only alternative to FSSH that has been able to address such excited state dynamics easily has been multiple spawning (110, 111). As the computational cost of excited state electronic structure is reduced in the future, the possible applications for surface hopping dynamics will grow rapidly.

6. DISCUSSION: DETAILED BALANCE, FRUSTRATED HOPS, TIME REVERSIBILITY

6.1. Detailed Balance

It is well known that an algorithm that preserves time reversibility should satisfy detailed balance (116). Here, by detailed balance we mean that, for any two weakly coupled systems (1, 2) with energies ϵ_1, ϵ_2 at temperature T, the equilibrium populations (N_1, N_2) should satisfy

$$\frac{N_2}{N_1} = e^{-(\epsilon_2 - \epsilon_1)/k_B T}. \tag{31}$$

Now, time reversibility is not a prerequisite for detailed balance. After all, Langevin dynamics are stochastic (and not time reversible), but Langevin dynamics obviously recover the correct equilibrium distribution for one surface. That being said, because surface hopping is stochastic and not time reversible, one can ask whether or not surface hopping dynamics obey detailed balance between electronic states. Parandekar, Schmidt & Tully (58, 59) and Sherman & Corcelli (117) have shown that the answer is, for the most part, yes (at least approximately). The explanation is quite simple, and relies on the possibility of forbidden hops.

Consider one point in configuration space R and assume that the trajectories follow a thermalized distribution of momenta P. The hopping rate is proportional to the product of the derivative couplings times the momentum. Let us ignore, for the moment, the dependence of the hopping rate on the electronic amplitudes, $\vec{c}$. In such a case, all hops downward are allowed, but upward hops can be accepted only when allowed energetically (i.e., when the hops are not frustrated). Thus, we expect (for $\Delta\epsilon \equiv \epsilon_2 - \epsilon_1$):

$$\frac{N_2}{N_1} = \frac{k_{1\to 2}}{k_{2\to 1}} = \frac{\int_{P_{\min}}^{\infty} dP P \exp\left(\frac{-P^2}{2MkT}\right)}{\int_0^{\infty} dP P \exp\left(\frac{-P^2}{2MkT}\right)} = \exp\left(\frac{-P_{\min}^2}{2MkT}\right) = \exp\left(-\frac{\Delta\epsilon}{kT}\right). \tag{32}$$

The argument above is rather robust. The only hiccups are that:

- The hopping rate depends on the electronic amplitudes, $\vec{c}$, which need not be symmetric for upward and downward hops.
- The momenta need not be thermalized in the presence of hops.

In practice, these caveats have only a limited effect; in general, FSSH does approximately recover the correct detailed balance at equilibrium (58, 59, 117). When decoherence is included, we have found that these conclusions are unchanged (B.R. Landry and J.E. Subotnik, unpublished data).

6.2. Time Reversibility

Given that, empirically, the FSSH algorithm approximately satisfies detailed balance, one might then wonder about the time reversibility of the FSSH algorithm. Obviously, each FSSH trajectory is stochastic and not strictly time reversible; in fact, there is no stable algorithm that can rigorously invert FSSH trajectories in time (118). That being the case, there is a less strenuous measure of time reversibility that one can contemplate. Consider the avoided crossing problem in **Figure 6*a*** and suppose a particle can enter from the left (l) or from the right (r) on the lower surface. In principle, by time reversibility, one should find symmetric transmission coefficients: $T_{l\to r}(E) = T_{r\to l}(E)$ (119). In practice, one can wonder whether surface hopping obeys this equality (at least approximately).

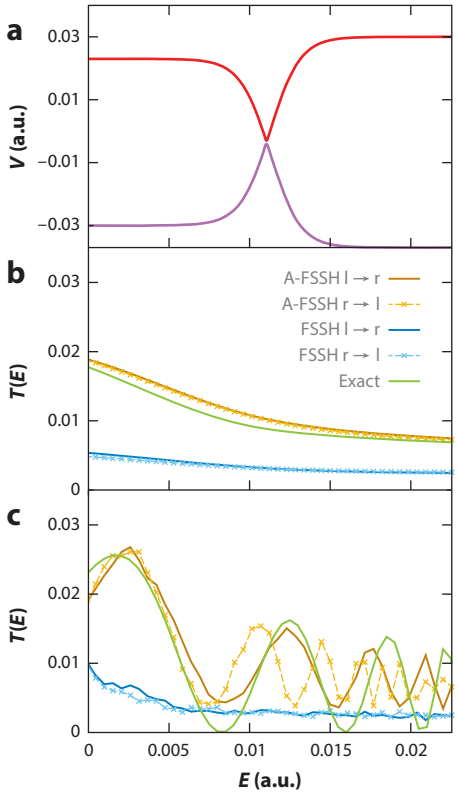

Figure 6

Transmission coefficients (T) for scattering in the limit of very small diabatic coupling. (*a*) The potential energy surfaces as a function of position; the particle is incoming on the lower adiabat. (*b*) The transmission coefficients averaged over an energy width of 0.005 a.u., corresponding to an incoming wavepacket. Note that the A-FSSH calculations are very close to the exact results, whereas the FSSH calculations are off by approximately a factor of 2; for more details, see Reference 120. (*c*) Transmission coefficients $T(E)$ without any averaging. Note that the A-FSSH values are similar for left-to-right (l → r) and right-to-left (r → l) scattering; time reversal symmetry would require that they be exactly equal. In contrast to **Figure 2*c***, note that A-FSSH (with decoherence) now correctly show oscillations in transmission as a function of energy, whereas FSSH calculations (without decoherence) do not show any such oscillations in transmission.

Figure 6 answers this question partially in the limit of very small diabatic coupling. In **Figure 6*b***, we show transmission rates averaged over an energy width of 0.005 a.u., corresponding to a wavepacket rather than a plane wave. This data proves empirically that, for a one-dimensional asymmetric curve crossing problem, both A-FSSH and FSSH do satisfy $T_{l\to r}(E) \approx T_{r\to l}(E)$ approximately (for more details, see Reference 120). Note that, with decoherence, A-FSSH is much closer to the final result. In **Figure 6*c***, we show an interesting nuance: Without decoherence, there are no oscillations in the transmission function $T(E)$ for the FSSH algorithm. By contrast, with decoherence, A-FSSH actually picks up such oscillations (which do exist, according to an exact calculation). This difference directly contradicts the intuition we gained above (in Section 3.1, **Figure 2**). Therefore, one must conclude that the effects of decoherence are not always obvious and that identifying the decoherence failures of a FSSH calculation retrospectively might also not necessarily be simple.

6.3. Momentum Reversal and Scaling in the Nonadiabatic Marcus Regime

There is one final detail that must now be discussed regarding forbidden hops and detailed balance, namely the notion of reversing momenta. Although detailed balance demands the presence of forbidden hops, over the years, several authors have suggested the possibility of reversing velocities in the direction of the derivative coupling after a forbidden hop (52, 121, 122). Some authors have favored velocity reversal (121, 122), and some have not (52). Recently, Jasper & Truhlar (12, 123) performed arguably the most comprehensive studies on the subject in the gas phase and proposed that velocity reversal should be applied, but only when the excited state has a gradient opposing the trajectory's velocity; this is called the grad V method (12).

With this background in mind, **Figure 7** shows an interesting feature. In this plot, we return to the spin-boson model. For small diabatic coupling (V_c), the dynamics are in the nonadiabatic Marcus regime; for larger diabatic couplings, the dynamics are in the adiabatic Marcus regime (96, 124). **Figure 7** shows that, without velocity reversal, the A-FSSH algorithm still does not recover the correct V_c^2 scaling in the limit of small diabatic coupling (V_c) if the friction is not too large. By contrast, with velocity reversal (according to the grad V ansatz), the A-FSSH algorithm recovers the correct V_c^2 scaling exactly (for more details, see Reference 93). Thus, velocity reversal would appear to be an essential element of the surface hopping algorithm going forward, which is also consistent with maintaining detailed balance.

7. CONCLUSIONS AND FUTURE DIRECTIONS

In this article, we have attempted to give an overview of recent progress and excitement in the field of surface hopping. Surface hopping trajectories have been used for decades (10, 127), and we have argued that many of the original questions about the FSSH algorithm have been resolved. For example, lingering questions of decoherence and initialization are now mostly answered. The result is that one can usually use independent surface hopping trajectories to capture nonadiabatic effects safely and efficiently (without relying on phase cancellation).

We must emphasize that this review is not comprehensive. On the one hand, we have not included many recent methodological developments. These developments include:

- formalisms for treating spectroscopy and FSSH consistently (86–88, 128–132);
- formalisms for incorporating finite shape pulses (133–135);
- formalisms for generating rate constants with FSSH (93, 120, 136);
- formalisms for propagating surface hopping dynamics with a continuum of states (137), e.g., near a metal surface (138–141);
- formalisms for solving the so-called trivial crossing problem that arises when one runs FSSH with many, many electronic states (99, 142–146); and
- formalisms for surface hopping beyond the FSSH algorithm that include some complex phase cancellation (147, 148).

On the other hand, it is our hope that this review will be of help to those confused graduate students who wish to run nonadiabatic dynamics calculations in the condensed phase and who want to understand their simulations.

Given that there are so many interesting, nonadiabatic problems in photochemistry that require a detailed theoretical treatment, we expect that the future will witness only more applications of surface hopping techniques (likely on both semi-empirical and ab initio electronic surfaces).

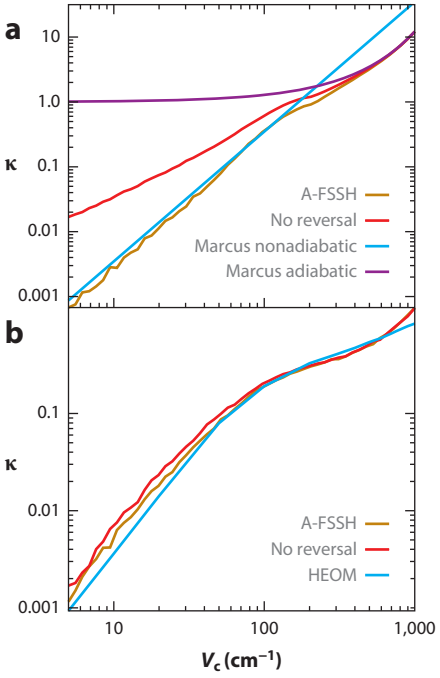

Figure 7

Transmission coefficients (κ) for electron transfer with a spin-boson system as a function of diabatic coupling V_c; κ is proportional to the rate. (*a*) The transition state estimate of κ without friction. Notice that A-FSSH correctly interpolates between the nonadiabatic and adiabatic Marcus rates, but reversing velocities with frustrated hops is essential (see *red line*). (*b*) The transmission coefficient κ with large friction. Notice that A-FSSH recovers the exact hierarchical equation of motion (HEOM) (125, 126) rate. All surface hopping calculations here were performed with transition state theory (as opposed to direct dynamics); errors for large V_c and large friction in panel *b* do not reflect incorrect dynamics but rather the limitations of transition state theory with small barriers. For more details, see Reference 93.

8. APPENDIX: EARLY DECOHERENCE CORRECTIONS

For aficionados of decoherence, we provide here a few more details about early decoherence corrections for FSSH. Consider two frozen Gaussians with centers labeled 1 and 2. Their overlap is

$$|S(t)| = \exp\left(\sum_\alpha \frac{-1}{4a_{R_\alpha}^2}\left(R_1^\alpha(t) - R_2^\alpha(t)\right)^2\right)\exp\left(\sum_\alpha \frac{-1}{4a_{P_\alpha}^2}\left(P_1^\alpha(t) - P_2^\alpha(t)\right)^2\right),$$

where a_R^2 is twice the width of the wavepacket in coordinate space: $2\cdot(\langle R^2\rangle - \langle R\rangle^2)$.

Originally, when Rossky, Bittner, Schwartz & Prezhdo (36, 37) derived their decoherence rate, they did so by modeling two frozen Gaussians with the same instantaneous position and momentum at time zero and then calculating the overlap between Gaussians to the second order in time. They arrived at the decoherence rate

$$\frac{1}{\tau_d} = \frac{\sqrt{\sum_\alpha \left(F_{11}^\alpha - F_{22}^\alpha\right)^2 a_{R_\alpha}^2}}{2\hbar}. \tag{33}$$

Later, Jasper & Truhlar (49) noticed that, if one does not assume that the frozen Gaussians have the same position and momentum, their overlap decays at first order in time, leading to a decoherence rate of the form

$$\frac{1}{\tau_d} = \sum_\alpha \frac{1}{2a_{P_\alpha}^2}\Big(P_1^\alpha(0) - P_2^\alpha(0)\Big)\Big(F_1^\alpha(0) - F_2^\alpha(0)\Big) + \sum_\alpha \frac{1}{2M_\alpha a_{R_\alpha}^2}\Big(R_1^\alpha(0) - R_2^\alpha(0)\Big)\Big(P_1^\alpha(0) - P_2^\alpha(0)\Big). \quad (34)$$

Thus, the Jasper–Truhlar approach is not strictly proportional to $\Delta\vec{F}$; there is another term that depends only on position and momentum difference.

On the one hand, it is clear that Truhlar & Jasper were correct that the decoherence rate is dominated by first-order rather than second-order terms: Why should there not be a first-order term? Indeed, our current understanding of decoherence (see Equations 23–26) is that one must search for nonlocal information; the width of the wavepacket is not enough for a decoherence correction, as Equation 33 would suggest. Our A-FSSH algorithm is predicated on the idea of trying to compute the factors $\vec{P}_2 - \vec{P}_1$ in Equation 34 (42, 43). On the other hand, Rossky and coworkers were correct that the decoherence rate should be proportional to $\Delta\vec{F}$. The second term in Equation 34 is tied strictly to the frozen Gaussian ansatz and is not physical. After all, there is no decoherence between wavepackets on parallel surfaces and it is not a coincidence that no such decoherence (proportional to a velocity difference only) arises when we analyze FSSH in the context of the QCLE (as in Section 4.1).

As a side note, Zhu & Truhlar (149, 150) long ago proposed using the adiabatic energy gap ΔV as a time scale for decoherence: $1/\tau_d \propto \hbar/\Delta V$. This premise was later implemented and advocated by Granucci and coworkers (151) and became yet another, somewhat popular, time scale for decoherence (102, 152). However, because this time scale is not proportional to $\Delta\vec{F}$, it is unclear how such an approach can be justified beyond a frozen Gaussian ansatz; after all, there is no decoherence at all between wavepackets on parallel surfaces. In practice, we have shown that the decoherence scheme in Reference 151 does not successfully reproduce the branching ratios for Tully's problem 2 (153). Moreover, it would appear unlikely that such an approach could recover Redfield theory (154) in the limit of very small reorganization energies, even though Redfield theory can be recovered easily simply by integrating the time-dependent electronic Schrödinger equation on almost any surface and ignoring classical feedback.

DISCLOSURE STATEMENT

The authors are not aware of any affiliations, memberships, funding, or financial holdings that might be perceived as affecting the objectivity of this review.

ACKNOWLEDGMENTS

J.E.S. thanks Neil Shenvi, Sharon Hammes-Schiffer, Todd Martínez, and John Tully for many interesting and insightful discussions over the years. This material is based on work supported by the (US) Air Force Office of Scientific Research (USAFOSR) PECASE award under AFOSR Grant FA9950-13-1-0157. J.E.S. acknowledges a Cottrell Research Scholar Fellowship and a David and Lucile Packard Fellowship.

LITERATURE CITED

1. Closs GL, Piotrowiak P, MacInnis JM, Fleming GR. 1988. Determination of long distance intramolecular triplet energy-transfer rates. Quantitative comparison with electron transfer. *J. Am. Chem. Soc.* 110:2652–53
2. Closs GL, Johnson M, Miller JR, Piotrowiak P. 1989. A connection between intramolecular long-range electron, hole, and triplet energy transfers. *J. Am. Chem. Soc.* 111:3751–53
3. Landry BR, Subotnik JE. 2014. Quantifying the lifetime of triplet energy transfer processes in organic chromophores: a case study of 4-(2-naphthylmethyl)benzaldehyde. *J. Chem. Theory Comp.* 10:4253–63
4. Lengsfield BH, Yarkony DR. 1992. Nonadiabatic interactions between potential energy surfaces: theory and applications. *Adv. Chem. Phys.* 82(Part 2):1–71
5. Lengsfield BH, Saxe P, Yarkony DR. 1984. On the evaluation of nonadiabatic coupling matrix elements using SA-MCSCF/CI wave functions and analytic gradient methods. I. *J. Chem. Phys.* 81:4549–53
6. Li X, Tully JC, Schlegel HB, Frisch MJ. 2005. Ab initio Ehrenfest dynamics. *J. Chem. Phys.* 123:084106
7. Cotton SJ, Igumenshchev K, Miller WH. 2014. Symmetrical windowing for quantum states in quasi-classical trajectory simulations: application to electron transfer. *J. Chem. Phys.* 141:084104
8. Martínez TJ, Ben-Nun M, Levine RD. 1996. Multi-electronic-state molecular dynamics: a wave function approach with applications. *J. Phys. Chem.* 100:7884–95
9. Ben-Nun M, Martínez TJ. 2000. A multiple spawning approach to tunneling dynamics. *J. Chem. Phys.* 112:6113–21
10. Tully JC. 1990. Molecular dynamics with electronic transitions. *J. Chem. Phys.* 93:1061–71
11. Malhado JP, Bearpark MJ, Hynes JT. 2014. Non-adiabatic dynamics close to conical intersections and the surface hopping perspective. *Front. Chem.* 2:97
12. Jasper AW, Truhlar DG. 2011. Non-Born–Oppenheimer molecular dynamics for conical intersections, avoided crossings, and weak interactions. In *Conical Intersections: Theory, Computation and Experiment*, ed. W Domcke, DR Yarkony, H Koppel, pp. 375–414. New Jersey: World Sci.
13. Barbatti M. 2011. Nonadiabatic dynamics with trajectory surface hopping method. *Wiley Interdiscip. Rev. Comput. Mol. Sci.* 1:620–33
14. Doltsinis N. 2002. Nonadiabatic dynamics: mean-field and surface hopping. In *Quantum Simulations of Complex Many-Body Systems: From Theory to Algorithms*, ed. J Grotendorst, D Marx, A Muramatsu, pp. 377–97. Jülich, Germany: John von Neumann Inst. Comput.
15. Coker DF. 1993. Computer simulation methods for nonadiabatic dynamics in condensed systems. In *Computer Simulation in Chemical Physics*, ed. MP Allen, DJ Tildesley, pp. 315–78. Jülich, Germany: John von Neumann Inst. Comput.
16. de Carvalho FF, Bouduban MEF, Curchod BFE, Tavernelli I. 2014. Nonadiabatic molecular dynamics based on trajectories. *Entropy* 16:62–85
17. Makri N, Makarov DE. 1995. Tensor propagator for iterative quantum time evolution of reduced density matrices. I. Theory. *J. Chem. Phys.* 102:4600–10
18. Makri N, Makarov DE. 1995. Tensor propagator for iterative quantum time evolution of reduced density matrices. II. Numerical methodology. *J. Chem. Phys.* 102:4611–18
19. Tanimura Y. 2012. Reduced hierarchy equations of motion approach with Drude plus Brownian spectral distribution: probing electron transfer processes by means of two-dimensional correlation spectroscopy. *J. Chem. Phys.* 137:22A550
20. Bittner ER. 2000. Quantum tunneling dynamics using hydrodynamic trajectories. *J. Chem. Phys.* 112:9703–10
21. Miller WH. 2001. The semiclassical initial value representation: a potentially practical way for adding quantum effects to classical molecular dynamics simulations. *J. Phys. Chem. A* 105:2942–55
22. Miller WH. 2012. Perspective: quantum or classical coherence? *J. Chem. Phys.* 136:210901
23. Makri N, Thompson K. 1998. Semiclassical influence functionals for quantum systems in anharmonic environments. *Chem. Phys. Lett.* 291:101–9
24. Herman MF, Kluk E. 1984. A semiclassical justification for the use of non-spreading wavepackets in dynamics calculations. *Chem. Phys.* 91:27–34

25. Kay KG. 1994. Integral expressions for the semiclassical time dependent propagator. *J. Chem. Phys.* 100:4377–92
26. Meyer HD, Miller WH. 1979. A classical analog for electronic degrees of freedom in nonadiabatic collision processes. *J. Chem. Phys.* 70:3214–23
27. Meyer HD, Miller WH. 1980. Analysis and extension of some recently proposed classical models for electronic degrees of freedom. *J. Chem. Phys.* 72:2272–81
28. Stock G, Thoss M. 1997. Semiclassical description of nonadiabatic quantum dynamics. *Phys. Rev. Lett.* 78:578
29. Miller WH. 2009. Electronically nonadiabatic dynamics via semiclassical initial value methods. *J. Phys. Chem. A* 113:1405–15
30. Kim H, Nassimi A, Kapral R. 2008. Quantum-classical Liouville dynamics in the mapping basis. *J. Chem. Phys.* 129:084102
31. Nassimi A, Bonella S, Kapral R. 2010. Analysis of the quantum-classical Liouville equation in the mapping basis. *J. Chem. Phys.* 133:134115
32. Kim HW, Rhee YM. 2014. Improving long time behavior of Poisson bracket mapping equation: a non-Hamiltonian approach. *J. Chem. Phys.* 140:184106
33. Gherib R, Ryabinkin IG, Izmaylov AF. 2015. Why do mixed quantum-classical methods describe short-time dynamics through conical intersections so well? Analysis of geometric phase effects. *J. Chem. Theory Comp.* 11:1375–82
34. Schwartz BJ, Rossky PJ. 1994. Aqueous solvation dynamics with a quantum mechanical solute: computer simulation studies of the photoexcited hydrated electron. *J. Chem. Phys.* 101:6902–15
35. Bittner ER, Rossky PJ. 1995. Quantum decoherence in mixed quantum-classical systems: nonadiabatic processes. *J. Chem. Phys.* 103:8130–43
36. Schwartz BJ, Bittner ER, Prezhdo OV, Rossky PJ. 1996. Quantum decoherence and the isotope effect in condensed phase nonadiabatic molecular dynamics simulations. *J. Chem. Phys.* 104:5942–55
37. Prezhdo OV, Rossky PJ. 1997. Evaluation of quantum transition rates from quantum-classical molecular dynamics simulations. *J. Chem. Phys.* 107:5863–78
38. Wong KF, Rossky PJ. 2002. Dissipative mixed quantum-classical simulation of the aqueous solvated electron system. *J. Chem. Phys.* 116:8418–28
39. Wong KF, Rossky PJ. 2002. Solvent-induced electronic decoherence: configuration dependent dissipative evolution for solvated electron systems. *J. Chem. Phys.* 116:8429–38
40. Horenko I, Salzmann C, Schmidt B, Schutte C. 2002. Quantum-classical Liouville approach to molecular dynamics: surface hopping Gaussian phase-space packets. *J. Chem. Phys.* 117:11075–88
41. Subotnik JE, Shenvi N. 2011. Decoherence and surface hopping: When can averaging over initial conditions help capture the effects of wave packet separation? *J. Chem. Phys.* 134:244114
42. Subotnik JE, Shenvi N. 2011. A new approach to decoherence and momentum rescaling in the surface hopping algorithm. *J. Chem. Phys.* 134:024105
43. Landry BR, Subotnik JE. 2012. How to recover Marcus theory with fewest switches surface hopping: Add just a touch of decoherence. *J. Chem. Phys.* 137:22A513
44. Fang JY, Hammes-Schiffer S. 1999. Improvement of the internal consistency in trajectory surface hopping. *J. Phys. Chem. A* 103:9399–407
45. Fang JY, Hammes-Schiffer S. 1999. Comparison of surface hopping and mean field approaches for model proton transfer reactions. *J. Chem. Phys.* 110:11166–75
46. Bedard-Hearn MJ, Larsen RE, Schwartz BJ. 2005. Mean-field dynamics with stochastic decoherence (MF-SD): a new algorithm for nonadiabatic mixed quantum/classical molecular-dynamics simulations with nuclear-induced decoherence. *J. Chem. Phys.* 123:234106
47. Hack MD, Truhlar DG. 2001. Electronically nonadiabatic trajectories: continuous surface switching II. *J. Chem. Phys.* 114:2894–902
48. Volobuev YL, Hack MD, Topaler MS, Truhlar DG. 2000. Continuous surface switching: an improved time-dependent self-consistent-field method for nonadiabatic dynamics. *J. Chem. Phys.* 112:9716–26
49. Jasper AW, Truhlar DG. 2005. Electronic decoherence time for non-Born–Oppenheimer trajectories. *J. Chem. Phys.* 123:064103

50. Prezhdo OV, Rossky PJ. 1997. Mean-field molecular dynamics with surface hopping. *J. Chem. Phys.* 107:825–34
51. Tully JC. 1998. Mixed quantum-classical dynamics. *Faraday Discuss.* 110:407–19
52. Müller U, Stock G. 1997. Surface-hopping modeling of photoinduced relaxation dynamics on coupled potential-energy surfaces. *J. Chem. Phys.* 107:6230–45
53. Kelly A, Markland TE. 2013. Efficient and accurate surface hopping for long time nonadiabatic quantum dynamics. *J. Chem. Phys.* 139:014104
54. Hazra A, Soudackov AV, Hammes-Schiffer S. 2010. Role of solvent dynamics in ultrafast photoinduced proton-coupled electron transfer reactions in solution. *J. Phys. Chem. B* 114:12319–32
55. Schwerdtfeger CA, Soudackov AV, Hammes-Schiffer S. 2014. Nonadiabatic dynamics of electron transfer in solution: explicit and implicit solvent treatments that include multiple relaxation time scales. *J. Chem. Phys.* 140:034113
56. Landry BR, Subotnik JE. 2011. Standard surface hopping predicts incorrect scaling for Marcus golden-rule rate: The decoherence problem cannot be ignored. *J. Chem. Phys.* 135:191101
57. Fuji T, Suzuki YI, Horio T, Suzuki T, Mitri R, et al. 2010. Ultrafast photodynamics of furan. *J. Chem. Phys.* 133:234303
58. Parandekar PV, Tully JC. 2005. Mixed quantum-classical equilibrium. *J. Chem. Phys.* 122:094102
59. Schmidt JR, Parandekar PV, Tully JC. 2008. Mixed quantum-classical equilibrium: surface hopping. *J. Chem. Phys.* 129:044104
60. Landry BR, Falk MJ, Subotnik JE. 2013. Communication: the correct interpretation of surface hopping trajectories: how to calculate electronic properties. *J. Chem. Phys.* 139:211101
61. Worth GA, Bearpark MJ, Robb MA. 2005. Semiclassical nonadiabatic trajectory computations in photochemistry: Is the reaction path enough to understand a photochemical reaction mechanism? In *Computational Photochemistry*, ed. M Olivucci, pp. 171–90. Amsterdam: Elsevier
62. Berendsen HJC, Mavri J. 1995. Quantum dynamics simulation of a small quantum system embedded in a classical environment. In *Quantum Mechanical Simulation Methods for Studying Biological Systems*, ed. D Bicout, M Field, pp. 157–178. Berlin: Springer-Verlag
63. Martens CC, Fang JY. 1997. Semiclassical-limit molecular dynamics on multiple electronic surfaces. *J. Chem. Phys.* 106:4918–30
64. Donoso A, Martens CC. 1998. Simulation of coherent nonadiabatic dynamics using classical trajectories. *J. Phys. Chem. A* 102:4291–300
65. Kapral R, Ciccotti G. 1999. Mixed quantum-classical dynamics. *J. Chem. Phys.* 110:8919–29
66. Nielsen S, Kapral R, Ciccotti G. 2000. Mixed quantum-classical surface hopping dynamics. *J. Chem. Phys.* 112:6543–53
67. Aleksandrov IVZ. 1981. The statistical dynamics of a system consisting of a classical and a quantum subsystem. *Z. Naturforsch. A* 36:902–8
68. Boucher W, Traschen J. 1988. Semiclassical physics and quantum fluctuations. *Phys. Rev. D* 37:3522–32
69. Zhang WY, Balescu R. 1988. Statistical mechanics of a spin-polarized plasma. *J. Plasma Phys.* 40:199–213
70. Anderson A. 1995. Quantum back reaction on "classical" variables. *Phys. Rev. Lett.* 74:621–25
71. Prezhdo OV, Kisil VV. 1997. Mixing quantum and classical mechanics. *Phys. Rev. A* 56:162–75
72. Micha DA, Thorndyke B. 2002. Dissipative dynamics in many-atom systems: a density matrix treatment. *Int. J. Quant. Chem.* 90:759–771
73. Ouyang W, Subotnik JE. 2014. Estimating the entropy and quantifying the impurity of a swarm of surface-hopping trajectories: a new perspective on decoherence. *J. Chem. Phys.* 140:204102
74. Shi Q, Geva E. 2004. A derivation of the mixed quantum-classical Liouville equation from the influence functional formalism. *J. Chem. Phys.* 121:3393–404
75. Mukamel S. 1982. On the semiclassical calculation of molecular absorption and fluorescence spectra. *J. Chem. Phys.* 77:173–181
76. Shemetulskis NE, Loring RF. 1992. Semiclassical theory of the photon echo: applications to polar fluids. *J. Chem. Phys.* 97:1217–25
77. Egorov SA, Rabani E, Berne BJ. 1998. Vibronic spectra in condensed matter: a comparison of exact quantum mechanical and various semiclassical treatments for harmonic baths. *J. Chem. Phys.* 108:1407–22

78. Egorov SA, Rabani E, Berne BJ. 1999. Nonradiative relaxation processes in condensed phases: quantum versus classical baths. *J. Chem. Phys.* 110:5238–48
79. Bursulaya BD, Kim HJ. 1996. Effects of solute electronic structure variation on photon echo spectroscopy. *J. Phys. Chem.* 100:16451–56
80. Subotnik JE, Ouyang W, Landry BR. 2013. Can we derive Tully's surface-hopping algorithm from the semiclassical quantum Liouville equation: almost, but only with decoherence. *J. Chem. Phys.* 139:214107
81. Horsfield AP, Bowler DR, Fisher AJ, Todorov TN, Sanchez CG. 2004. Beyond Ehrenfest: correlated non-adiabatic molecular dynamics. *J. Phys. Cond. Matter* 16:8251–66
82. Stella L, Meister M, Fisher AJ, Horsfield AP. 2007. Robust nonadiabatic molecular dynamics for metals and insulators. *J. Chem. Phys.* 127:214104
83. McEniry EJ, Bowler DR, Dundas D, Horsfield AP, Sanchez CG, Todorov TN. 2007. Dynamical simulation of inelastic quantum transport. *J. Phys. Cond. Matter* 19:196201
84. Prezhdo O, Pereverzev YV. 2000. Quantized Hamilton dynamics. *J. Chem. Phys.* 113:6557–65
85. Onuchic JN, Wolynes PG. 1988. Classical and quantum pictures of reaction dynamics in condensed matter: resonances, dephasing, and all that. *J. Phys. Chem.* 92:6495–503
86. Petit AS, Subotnik JE. 2014. How to calculate linear absorption spectra with lifetime broadening using fewest switches surface hopping trajectories: a simple generalization of ground-state Kubo theory. *J. Chem. Phys.* 141:014107
87. Petit AS, Subotnik JE. 2014. Calculating time-resolved differential absorbance spectra for ultrafast pump–probe experiments with surface hopping trajectories. *J. Chem. Phys.* 141:154108
88. Petit AS, Subotnik JE. 2105. Appraisal of surface hopping as a tool for modeling condensed phase linear absorption spectra. *J. Chem. Theory Comp.* 11:4328–41
89. Tanimura Y, Kubo R. 1989. Time evolution of a quantum system in contact with a nearly Gaussian–Markovian noise bath. *J. Phys. Soc. Jpn.* 58:101–114
90. Ishizaki A, Fleming GR. 2009. Unified treatment of quantum coherent and incoherent hopping dynamics in electronic energy transfer: reduced hierarchy equation approach. *J. Chem. Phys.* 130:234111
91. Cline RE, Wolynes PG. 1987. Stochastic dynamic models of curve crossing phenomena in condensed phases. *J. Chem. Phys.* 86:3836–44
92. Warshel A, Hwang JK. 1986. Simulation of the dynamics of electron transfer reactions in polar solvents: semiclassical trajectories and dispersed polaron approaches. *J. Chem. Phys.* 84:4938–57
93. Jain A, Subotnik JE. 2015. Surface hopping, transition state theory, and decoherence. II. Thermal rate constants and detailed balance. *J. Chem. Phys.* 143:134107
94. Ben-Nun M, Martínez TJ. 2007. A continuous spawning method for nonadiabatic dynamics and validation for the zero temperature spin boson problem. *Isr. J. Chem.* 47:75–88
95. Chen H-T, Reichman DR. 2016. On the accuracy of surface hopping dynamics in condensed phase non-adiabatic problems. *J. Chem. Phys.* 144:094104
96. Xie W, Baj S, Zhu L, Shi Q. 2013. Calculation of electron transfer rates using mixed quantum classical approaches: nonadiabatic limit and beyond. *J. Phys. Chem. A* 117:6196–204
97. Zhu X, Yarkony DR. 2014. Fitting coupled potential energy surfaces for large systems: method and construction of a 3-state representation for phenol photodissociation in the full 33 internal degrees of freedom using multireference configuration interaction determined data. *J. Chem. Phys.* 140:024112
98. Sterpone F, Bedard-Hearn MJ, Rossky PJ. 2009. Nonadiabatic mixed quantum-classical dynamic simulation of π-stacked oligophenylenevinylenes. *J. Phys. Chem. A* 113:3427–30
99. Nelson T, Fernandez-Alberti S, Roitberg AE, Tretiak S. 2014. Nonadiabatic excited-state molecular dynamics: modeling photophysics in organic conjugated materials. *Acc. Chem. Res.* 47:1155–64
100. Plasser F, Crespo-Otero R, Pederzoli M, Pittner J, Lischka H, Barbatti M. 2014. Surface hopping dynamics with correlated single-reference methods: 9H-adenine as a case study. *J. Chem. Theory Comp.* 10:1395–405
101. Barbatti M, Paier J, Lischka H. 2004. Photochemistry of ethylene: a multireference configuration interaction investigation of the excited-state energy surfaces. *J. Chem. Phys.* 121:11614
102. Barbatti M, Granucci G, Persico M, Ruckenbauer M, Vazdar M, et al. 2007. The on-the-fly surface-hopping program system Newton-X: application to ab initio simulation of the nonadiabatic photodynamics of benchmark systems. *J. Photochem. Photobiol. A Chem.* 190:228–40

103. Subotnik JE, Alguire EC, Ou Q, Landry BR, Fatehi S. 2015. The requisite electronic structure theory to describe photoexcited nonadiabatic dynamics: nonadiabatic derivative couplings and diabatic electronic couplings. *Acc. Chem. Res.* 48:1340–50
104. Tavernelli I, Curchod BFE, Rothlisberger U. 2009. On nonadiabatic coupling vectors in time-dependent density functional theory. *J. Chem. Phys.* 131:196101
105. Hu C, Sugino O, Tateyama Y. 2009. All-electron calculation of nonadiabatic couplings from time-dependent density functional theory: probing with the Hartree–Fock exact exchange. *J. Chem. Phys.* 131:114101
106. Send R, Furche F. 2010. First-order nonadiabatic couplings from time-dependent hybrid density functional response theory: consistent formalism, implementation, and performance. *J. Chem. Phys.* 132:044107
107. Fatehi S, Alguire E, Shao Y, Subotnik JE. 2011. Analytical derivative couplings between configuration interaction singles states with built-in translation factors for translational invariance. *J. Chem. Phys.* 135:234105
108. Li Z, Liu W. 2014. First-order nonadiabatic coupling matrix elements between excited states: a Lagrangian formulation at the CIS, RPA, TD-HF, and TD-DFT levels. *J. Chem. Phys.* 141:014110
109. Zhang X, Herbert JM. 2014. Analytic derivative couplings for spin-flip configuration interaction singles and spin-flip time-dependent density functional theory. *J. Chem. Phys.* 141:064104
110. Martínez TJ. 1997. Ab initio molecular dynamics around a conical intersection: Li(2p) + H_2. *Chem. Phys. Lett.* 272:139–47
111. Martínez TJ, Levine RD. 1996. First-principles molecular dynamics on multiple electronic states: a case study of NaI. *J. Chem. Phys.* 105:6334–41
112. Ou Q, Fatehi S, Alguire E, Subotnik JE. 2014. Derivative couplings between TDDFT excited states obtained by direct differentiation in the Tamm–Dancoff approximation. *J. Chem. Phys.* 141:024114
113. Ou Q, Alguire E, Subotnik JE. 2015. Derivative couplings between time-dependent density functional theory excited states in the random-phase approximation based on pseudowavefunctions: behavior around conical intersections. *J. Phys. Chem. B* 119:7150–61
114. Alguire E, Ou Q, Subotnik JE. 2015. Calculating derivative couplings between time-dependent Hartree–Fock excited states with pseudo-wavefunctions. *J. Phys. Chem. B* 119:7140–49
115. Shao Y, Gan Z, Epifanovsky E, Gilbert AT, Wormit M, et al. 2015. Advances in molecular quantum chemistry contained in the Q-Chem 4 program package. *Mol. Phys.* 113:184–215
116. Mahan BH. 1975. Microscopic reversibility and detailed balance. An analysis. *J. Chem. Ed.* 52:299–302
117. Sherman MC, Corcelli SA. 2015. Thermal equilibrium properties of surface hopping with an implicit Langevin bath. *J. Chem. Phys.* 142:024110
118. Subotnik JE, Rhee YM. 2015. On surface hopping and time-reversal. *J. Phys. Chem. A* 119:990–95
119. Tannor D. 2006. *Introduction to Quantum Mechanics: A Time-Dependent Perspective*. Univ. Sci. Books
120. Jain A, Herman MF, Ouyang W, Subotnik JE. 2015. Surface hopping, transition state theory and decoherence. I. Scattering theory and time-reversibility. *J. Chem. Phys.* 143:134106
121. Hammes-Schiffer S, Tully J. 1994. Proton transfer in solution: molecular dynamics with quantum transitions. *J. Chem. Phys.* 101:4657–67
122. Coker DF, Xiao L. 1995. Methods for molecular dynamics with nonadiabatic transitions. *J. Chem. Phys.* 102:496–510
123. Jasper AW, Hack MD, Truhlar DG. 2001. The treatment of classically forbidden electronic transitions in semiclassical trajectory surface hopping calculations. *J. Chem. Phys.* 115:1804–16
124. Huo P, Miller TF, Coker DF. 2013. Communication: predictive partial linearized path integral simulation of condensed phase electron transfer dynamics. *J. Chem. Phys.* 139:151103
125. Strümpfer J, Schulten K. 2012. Open quantum dynamics calculations with the hierarchy equations of motion on parallel computers. *J. Chem. Theory Comp.* 8:2808–16
126. Strümpfer J, Schulten K. 2009. Light harvesting complex II B850 excitation dynamics. *J. Chem. Phys.* 131:225101
127. Tully JC, Preston RK. 1971. Trajectory surface hopping approach to nonadiabatic molecular collisions: the reaction of H^+ with D_2. *J. Chem. Phys.* 55:562–72

128. Tempelaar R, van der Vegte CP, Knoester J, Jansen TLC. 2013. Surface hopping modeling of two-dimensional spectra. *J. Chem. Phys.* 138:164106
129. Tempelaar R, Spano FC, Knoester J, Jansen TLC. 2014. Mapping the evolution of spatial exciton coherence through time-resolved fluorescence. *J. Phys. Chem. Lett.* 5:1505–10
130. Zimmermann T, Vanicek J. 2014. Efficient on-the-fly ab initio semiclassical method for computing time-resolved nonadiabatic electronic spectra with surface hopping or Ehrenfest dynamics. *J. Chem. Phys.* 141:134102
131. Dorfman KE, Fingerhut BP, Mukamel S. 2013. Broadband infrared and Raman probes of excited-state vibrational molecular dynamics: simulation protocols based on loop diagrams. *Phys. Chem. Chem. Phys.* 15:12348–59
132. Fingerhut BP, Dorfman KE, Mukamel S. 2014. Probing the conical intersection dynamics of the RNA base uracil by UV-pump stimulated-Raman-probe signals: ab initio simulations. *J. Chem. Theory Comp.* 10:1172–88
133. Martínez-Mesa A, Saalfrank P. 2015. Semiclassical modelling of finite-pulse effects on nonadiabatic photodynamics via initial condition filtering: the predissociation of NaI as a test case. *J. Chem. Phys.* 142:194107
134. Shen YC, Cina JA. 1999. What can short-pulse pump–probe spectroscopy tell us about Franck–Condon dynamics? *J. Chem. Phys.* 110:9793–806
135. Richter M, Marquetand P, González-Vázquez J, Sola I, González L. 2011. SHARC: ab initio molecular dynamics with surface hopping in the adiabatic representation including arbitrary couplings. *J. Chem. Theory Comp.* 7:1253–58
136. Hammes-Schiffer S, Tully JC. 1995. Nonadiabatic transition state theory and multiple potential energy surface molecular dynamics of infrequent events. *J. Chem. Phys.* 103:8528–37
137. Ouyang W, Dou W, Subotnik JE. 2015. Surface hopping with a manifold of electronic states. I. Incorporating surface-leaking to capture lifetimes. *J. Chem. Phys.* 142:084109
138. Shenvi N, Roy S, Tully JC. 2009. Nonadiabatic scattering at metal surfaces: independent electron surface hopping. *J. Chem. Phys.* 130:174107
139. Shenvi N, Roy S, Tully JC. 2009. Dynamical steering and electronic excitation in NO scattering from a gold surface. *Science* 326:829–32
140. Dou W, Nitzan A, Subotnik JE. 2015. Surface hopping with a manifold of electronic states. II. Application to the many-body Anderson–Holstein model. *J. Chem. Phys.* 142:084110
141. Dou W, Nitzan A, Subotnik JE. 2015. Surface hopping with a manifold of electronic states. III. Transients, broadening, and the Marcus picture. *J. Chem. Phys.* 142:234106
142. Granucci G, Persico M, Toniolo A. 2001. Direct semiclassical simulation of photochemical processes with semiempirical wave functions. *J. Chem. Phys.* 114:10608–15
143. Fernandez-Alberti S, Roitberg AE, Nelson T, Tretiak S. 2012. Identification of unavoided crossings in nonadiabatic photoexcited dynamics involving multiple electronic states in polyatomic conjugated molecules. *J. Chem. Phys.* 137:014512
144. Meek GA, Levine BG. 2014. Evaluation of the time-derivative coupling for accurate electronic state transition probabilities from numerical simulations. *J. Phys. Chem. Lett.* 5:2351–56
145. Wang L, Prezhdo OV. 2014. A simple solution to the trivial crossing problem in surface hopping. *J. Phys. Chem. Lett.* 5:713–19
146. Meek GA, Levine BG. 2014. Evaluation of the time-derivative coupling for accurate electronic state transition probabilities from numerical simulations. *J. Phys. Chem. Lett.* 5:2351–56
147. Herman MF. 1982. Generalization of the geometric optical series approach for non-adiabatic scattering problems. *J. Chem. Phys.* 76:2949–58
148. Gorshkov VN, Tretiak S, Mozyrsky D. 2013. Semiclassical Monte-Carlo approach for modelling non-adiabatic dynamics in extended molecules. *Nature* 4:2144
149. Zhu C, Nangia S, Jasper AW, Truhlar DG. 2004. Coherent switching with decay of mixing: an improved treatment of electronic coherence for non-Born–Oppenheimer trajectories. *J. Chem. Phys.* 121:7658–70
150. Zhu C, Jasper AW, Truhlar DG. 2005. Non-Born–Oppenheimer Liouville–von Neumann dynamics. Evolution of a subsystem controlled by linear and population-driven decay of mixing with decoherent and coherent switching. *J. Chem. Theory Comp.* 1:527–40

151. Granucci G, Persico M, Zoccante A. 2010. Including quantum decoherence in surface hopping. *J. Chem. Phys.* 133:134111
152. Xia SH, Xie BB, Fang Q, Cui G, Thiel W. 2015. Excited-state intramolecular proton transfer to carbon atoms: nonadiabatic surface-hopping dynamics simulations. *Phys. Chem. Chem. Phys.* 17:9687–97
153. Falk MJ, Landry BR, Subotnik JE. 2014. Can surface hopping sans decoherence recover Marcus theory? Understanding the role of friction in a surface hopping view of electron transfer. *J. Phys. Chem. B* 118:8108–17
154. Landry BR, Subotnik JE. 2015. Surface hopping outperforms secular Redfield theory when reorganization energies range from small to moderate (and nuclei are classical). *J. Chem. Phys.* 142:104102

Annual Review of
Physical Chemistry
Volume 67, 2016

Contents

Indexes

Errata

An online log of corrections to *Annual Review of Physical Chemistry* articles may be found at http://www.annualreviews.org/errata/physchem